

¹ **GLO-Roots: an imaging platform enabling multidimensional characterization of soil-grown roots systems**

³ Rubén Rellán-Álvarez^{1, 9}, Guillaume Lobet², Heike Lindner^{1, 8}, Pierre-Luc Pradier^{1, 8, 10},
⁴ Jose Sebastian^{1, 8}, Muh-Ching Yee¹, Yu Geng^{1, 7}, Charlotte Trontin¹, Therese LaRue³,
⁵ Amanda Schrager-Lavelle⁴, Cara H. Haney⁵, Rita Nieu⁶, Julin Maloof⁴, John P. Vogel⁷,
⁶ José R. Dinneny^{1, 12}

⁷ ¹ Department of Plant Biology, Carnegie Institution for Science, Stanford, CA, USA.

⁸ ² PhytoSystems, University of Liège, Liège, Belgium.

⁹ ³ Department of Biology, Stanford University, Stanford, CA, USA.

¹⁰ ⁴ Department of Plant Biology, UC Davis, Davis, CA, USA.

¹¹ ⁵ Harvard Medical School, Massachusetts General Hospital, Department of Genetics, De-
¹² partment of Molecular Biology Boston, MA, USA

¹³ ⁶ USDA Western Regional Research Center, Albany, CA, USA

¹⁴ ⁷ DOE Joint Genome Institute, Walnut Creek, CA, USA

¹⁵ ⁸ These authors contributed equally

¹⁶ ⁹ Present address: Laboratorio Nacional de Genómica para la Biodiversidad (Langebio),
¹⁷ Unidad de Genómica Avanzada, Centro de Investigación y de Estudios Avanzados del Insti-
¹⁸ tuto Politécnico Nacional (CINVESTAV-IPN), Irapuato, Guanajuato, México

¹⁹ ¹⁰ Present address: Boyce Thompson Institute for Plant Research/USDA, Ithaca, NY, USA.

²⁰ ¹¹ Present address: Energy Biosciences Institute, UC, Berkeley, CA, USA

²¹ ¹² Corresponding author

²² **Author contributions:**

²³ RR-A: Conception, design and development of the growth and imaging system and Arabidop-
²⁴ sis transgenic lines; acquisition, analysis and interpretation of data; drafting and revising

25 the article.

26 GL: Development of the GLO-RIA image analysis plugin, analysis and interpretation of

27 data, drafting and revising the article.

28 HL: Acquisition of data, development of the tomato growth and imaging setup.

29 P-LP: Acquisition of data, analysis and interpretation of data

30 JS: Development of Brachypodium transgenic lines, acquisition and analysis of Brachy-

31 podium, Arabidopsis and tomato data.

32 MCY: Development of Arabidopsis and Brachypodium transgenic lines.

33 YG: Development of Arabidopsis transgenic lines.

34 CT: Acquisition and analysis of the QPCR data

35 TL: Acquisition and analysis of the QPCR data

36 AS-L: Contributed the unpublished dual-color tomato line.

37 CH: Contributed the unpublished *Pseudomonas fluorescens* CH267-lux strain.

38 RN: Contribution to the development of the Brachypodium transgenic line.

39 JM: Contributed the unpublished dual-color tomato line.

40 JPV: Contribution to the development of the Brachypodium transgenic line.

41 JRD: Conception, design and development of the growth and imaging system and Arabidop-

42 sis transgenic lines; acquisition, analysis and interpretation of data; drafting and revising

43 the article.

44 All authors read and approve the final version of the manuscript.

45 **Abstract**

46 Root systems develop different root types that individually sense cues from their local

47 environment and integrate this information with systemic signals. This complex multi-

48 dimensional amalgam of inputs enables continuous adjustment of root growth rates, direc-
49 tion and metabolic activity that define a dynamic physical network. Current methods for
50 analyzing root biology balance physiological relevance with imaging capability. To bridge
51 this divide, we developed an integrated imaging system called Growth and Luminescence
52 Observatory for Roots (GLO-Roots) that uses luminescence-based reporters to enable stud-
53 ies of root architecture and gene expression patterns in soil-grown, light-shielded roots. We
54 have developed image analysis algorithms that allow the spatial integration of soil prop-
55 erties such as soil moisture with root traits. We propose GLO-Roots as a system that
56 has great utility in presenting environmental stimuli to roots in ways that evoke natural
57 adaptive responses and in providing tools for studying the multi-dimensional nature of such
58 processes.

59 **Introduction**

60 Plant roots are three-dimensional assemblies of cells that coordinately monitor and acclimate
61 to soil environmental change by altering physiological and developmental processes through
62 cell-type and organ-specific regulatory mechanisms^{1,2}. Soil comprises a complex distribution
63 of particles of different size, composition and physical properties, airspaces, variation in
64 nutrient availability and microbial diversity^{3,4}. These physical, chemical and biological
65 properties of soil can vary on spatial scales of meters to microns, and on temporal scales
66 ranging from seasonal change to seconds. Root tips monitor this environment through
67 locally and systemically acting sensory mechanisms^{5,6}.

68 The architecture of the root system determines the volume of soil where resources can be
69 accessed by the plant (rhizosphere) and is under both environmental and genetic control.
70 Plasticity in growth parameters allows the plant to adjust its form to suit a particular soil.
71 Lateral roots, which usually make up the majority of the total root system, often grow at an
72 angle divergent from the gravity vector. This gravity set-point angle (GSA) is controlled by
73 auxin biosynthesis and signaling and can be regulated by developmental age and root type⁷.
74 Recent cloning of the *DRO1* Quantitative Trait Locus (QTL) demonstrates that natural

75 genetic variation is a powerful tool for uncovering such control mechanisms⁸.

76 Specific root ideotypes (idealized phenotypes) have been proposed to be optimal for acquisi-
77 tion of water and nitrogen, which are distinct from ideotypes for low phosphorus. Based on
78 computational modeling and field studies, the “steep, deep and cheap” ideotype proposed by
79 Lynch and colleagues may provide advantages to the plant for capturing water and elements
80 like nitrogen that are water soluble and therefore tend to move in the soil column with water.
81 This ideotype consists of highly gravitropic, vertically oriented roots that grow deep in the
82 soil column and develop large amounts of aerenchyma, which reduces the overall metabolic
83 cost of the root system³. Other nutrients, like phosphorus, which have limited water solu-
84 bility and are tightly bound to organic matter, usually accumulate in the top layers of soil
85 and favor root systems that are more highly branched and shallow. The low-phosphorus
86 ideotype effectively increases root exploration at the top layers of soil³. Modeling of root
87 system variables shows that optimum architecture for nitrogen and phosphorus uptake are
88 not the same⁹ and suggests tradeoffs that may affect the evolution of root architecture as a
89 population adapts to a particular environmental niche.

90 Clearly, understanding the architecture of root systems and how environmental conditions
91 alter root developmental programs is important for understanding adaptive mechanisms of
92 plants and for identifying the molecular-genetic basis for different response programs. In
93 addition, root systems have complexity beyond their architecture that needs to be incorpo-
94 rated into our understanding of plant-environment interactions. Primary and lateral roots
95 exhibit different stress response programs in *Arabidopsis*² and may play specialized roles
96 in water and nutrient uptake. Thus, it is important to develop methods that allow for a
97 multidimensional characterization of the root system that includes growth, signaling, and
98 interactions with other organisms. Furthermore, physiological parameters that affect whole
99 plant responses to the environment, such as transpiration, are likely integrated into such
100 processes, thus requiring a more holistic approach to studies of root function.

101 Based on these considerations we have developed a new root imaging platform, Growth
102 and Luminescence Observatory for Roots (GLO-Roots), which allows root architecture and

103 gene expression to be studied in soil-grown plants. GLO-Roots is an integrated system
104 composed of custom growth vessels, luminescent reporters and imaging systems. We use
105 rhizotrons that have soil volumes equivalent to small pots and support growth of Arabidopsis
106 from germination to senescence. To visualize roots, we designed plant-codon optimized
107 luciferase reporters that emit light of different wavelengths. To visualize reporter expression,
108 plants are watered with a dilute luciferin solution and imaged afterwards. We have built
109 a custom luminescence imaging system that automatically captures images of rhizotrons
110 held vertically. The signal from each reporter is distinguished using band-pass filters held
111 in a motorized filter wheel, which enables automated acquisition of images from plants
112 expressing both structural and environmentally and developmentally responsive reporters.
113 We have also developed GLO-RIA (GLO-Roots Image Analysis), an ImageJ¹⁰ plugin that
114 allows for automated determination of root system area, convex hull, depth, width and
115 directionality, which quantifies the angle of root segments with respect to gravity. GLO-
116 RIA is also able to relate root system parameters to local root-associated variables such as
117 reporter expression intensity and soil-moisture content.

118 Overall GLO-Roots has great utility in presenting environmental stimuli to roots in phys-
119 iologically relevant ways and provides tools for characterizing responses to such stimuli at
120 the molecular level in whole adult root systems over broad time scales.

121 **Box 1.**

122 All resources for GLO-Roots, including the original raw data used in the manuscript, sample
123 images, GLO-RIA user manual, the latest software updates and the source code, can be
124 found at: <https://dinnenylab.wordpress.com/glo-roots/>

125 **Results**

126 We have developed an integrated platform for growing, imaging and analyzing root growth
127 that provides advances in physiological relevance and retains the ability to visualize aspects

¹²⁸ of root biology beyond structure.

¹²⁹ **The GLO-Roots platform**

¹³⁰ GLO-Roots is comprised of four parts: i) growth vessels called rhizotrons that allow plant
¹³¹ growth in soil and root imaging; ii) luminescent reporters that allow various aspects of root
¹³² biology to be tracked in living plants; iii) GLO1 luminescence-imaging system designed to
¹³³ automatically image rhizotrons; iv) GLO-RIA, an image analysis suite designed to quantify
¹³⁴ root systems imaged using GLO-Roots.

¹³⁵ **Plant growth system** GLO-Roots utilizes custom designed growth vessels classically
¹³⁶ known as rhizotrons, which hold a thin volume of soil between two sheets of polycarbonate
¹³⁷ plastic. Acrylic spacers provide a 2-mm space in which standard peat-based potting mix
¹³⁸ is added. Black vinyl sheets protect roots from light and rubber U-channels clamp the
¹³⁹ rhizotron materials together. Plastic racks hold the rhizotrons vertically and further protect
¹⁴⁰ the roots from light. Rhizotrons and rack are placed in a black tub and water are added, to
¹⁴¹ a depth of about 2 cm, at the bottom to maintain moisture in the rhizotrons during plant
¹⁴² growth. The volume of soil in the rhizotrons (100 cm^3) is similar to small pots commonly
¹⁴³ used for Arabidopsis and supports growth throughout the entire life cycle (Fig 1A-C and
¹⁴⁴ Supplement 1).

¹⁴⁵ To determine how the biology of plants grown in rhizotrons compares to other standard
¹⁴⁶ growth systems, we utilized high-throughput qRT-PCR to study how these conditions af-
¹⁴⁷ fect expression of 77 marker genes in root and shoot samples. These genes were curated
¹⁴⁸ from the literature and belong to a wide array of biological pathways including nutrient
¹⁴⁹ acquisition, hormone and light response and abiotic stress. Whole roots and shoot samples
¹⁵⁰ were collected at the end of the light and dark periods (Long-day conditions: 16 hour light,
¹⁵¹ 8 hours dark) from plants grown in rhizotrons, pots, and petri dishes with two different me-
¹⁵² dia compositions (1X Murashige and Skoog basal salts (MS), 1% sucrose or 0.25X MS, no
¹⁵³ sucrose). Principal component analysis of the gene expression values showed a separation of

soil and gel-grown root systems in the the first principal components (Figure 1-figure supplement 1A). We observed enhanced expression of genes associated with light-regulated pathways (flavonoid biosynthesis: *FLAVINOL SYNTHASE1*, *FLS1*, *CHALCONE SYNTHASE*, *CHS*), (photosynthesis: *RUBISCO SUBUNITS1A*, *RBCS1A CYCLOPHILIN 38*, *CYP38*), which is expected due to the exposure of gel-grown roots to light. In addition, genes associated with phosphorus nutrition (*LOW PHOSPHATE RESPONSE1*, *LPR1*, *PHOSPHATE STARVATION RESPONSE1*, *PHR1*) were among others (Figure 1-figure table supplement 1) expressed predominantly in soil-grown roots, suggesting differences in nutrient availability between the different growth systems. Interestingly, shoot samples where not clearly distinguished by growth media and, instead, time of day had a greater effect (Figure 1-Supplement 2). These data suggest root systems may be particularly sensitive to media conditions and indicate that rhizotron-grown root systems more closely approximate the biology of pot-grown plants than standard gel-based media. Shoot weight and primary root length were significantly reduced for gel-grown plants compared to rhizotron- or pot-grown plants suggesting significant differences in the biology of plants grown under these conditions (Figure 1-figure supplement 1B-C). While the 2 mm depth of the soil sheet is 10 to 20 times the average diameter of an Arabidopsis root (between 100-200 microns¹¹), we evaluated whether rhizotron-grown plants exhibited any obvious stress as a consequence of physical constriction. We compared traits of plants growing in vessels that hold similar volumes of soil but in different volumetric shapes. The number of lateral roots was significantly lower in pot and cylinder-grown plants compared to rhizotron-grown plants (Figure 1-figure supplement 1D) whereas primary root length of rhizotron and cylinder-grown plants was significantly greater than pot-grown plants (Figure 1-figure supplement 1E). No significant differences in shoot area were observed between the three systems (Figure 1-figure supplement 1-data). Thus, these data do not support the hypothesis that rhizotron-grown plants experience physical constriction greater than other vessels holding the same volume of soil.

Generation of transgenic plants expressing different luciferases Arabidopsis roots cannot easily be distinguished from soil using brightfield imaging due to their thinness and

translucency (Figure 1-figure supplement 3); thus, reporter genes are needed to enhance the contrast between the root and their environment. Luciferase is an ideal reporter to visualize roots: 1) unlike fluorescent reporters, luciferase does not require high-intensity excitation light, which could influence root growth, 2) peat-based soil (a type of histosol) exhibits no autoluminescence but does autofluoresce at certain excitation wavelengths similar to GFP (Figure 1-figure supplement 3), 3) while GFP is very stable, and thus not as suitable for imaging dynamic transcriptional events, the luciferase enzyme is inactivated after catabolism of luciferin, making it ideal for studying processes such as environmental responses. A considerable number of luciferases have been developed that emit light spanning different regions of the visible spectrum, but their utilization has been limited to studies in animals (Table 1).

To determine the efficacy of using luciferase to visualize roots in soil, we codon optimized sequences of *PpyRE8*, *CBGRed*, *LUC2*, and *CBG99* for Arabidopsis expression. In addition, nanoLUC and venus-LUC²¹² were utilized. Constitutive luciferase expression was driven in plants using the *UBIQUITIN 10* (*UBQ10*) or *ACTIN2* (*ACT2*) promoters using vectors assembled through a Golden-Gate cloning system¹³. Plants homozygous for a single locus T-DNA insertion were evaluated for in vivo emission spectra and luminescence intensity (Fig 1D). All the evaluated luciferases use D-luciferin as a substrate facilitating the simultaneous imaging of different luciferases except nanoLUC, which uses a proprietary substrate furimazine¹⁴. In general, luciferases with red-shifted emission spectra were less intense than the green-shifted luciferases (Fig 1D). LUC2o showed an emission maximum at 580 nm and a minor peak at 620 nm while CBG99o lacks the minor peak.

Continuous addition of luciferin did not have any significant effect on shoot weight or primary root length (Figure 1-figure supplement 4). After luciferin addition, luminescence signal could be reliably detected in root systems for up to 10 days, depending on the developmental state of the plant.

208 **GLO1: a semi-automated luminescence imaging system for rhizotrons** Lumines-
209 cence imaging systems commercially available for biomedical research are usually optimized
210 for imaging horizontally held specimens or samples in microtiter plates. Placing rhizotrons
211 in this position would induce a gravitropic response in plants. Working with Bioimaging
212 Solutions (San Diego, CA) we designed and built a luminescence imaging system optimized
213 for rhizotron-grown plants. GLO1 (Growth and Luminescence Observatory 1) uses two
214 back-thinned CCD cameras (Princeton Instruments, USA) to capture partially-overlapping
215 images of rhizotrons while a motorized stage automatically rotates the rhizotron to capture
216 images of both sides (Fig 1E). A composite image is generated from the images captured
217 of each side; Fig 1F shows that approximately half of the root system is revealed on each
218 side with few roots being visible on both sides. Apparently, the soil sheet is thick enough
219 to block portions of the root system but thin enough to ensure its continuous structure
220 can be compiled from opposite face views. We tested the ability of GLO1-generated images
221 to reveal complete root systems by manually quantifying the number of lateral roots in
222 excavated root systems of 8 different plants and testing these results against estimates of
223 lateral root number from images of the same plants visually inspected by 4 different per-
224 sons. These comparisons revealed good correlation ($(R^2 = 0.974)$) between actual lateral
225 root counts and image-based estimation, indicating GLO1-generated root images provide
226 an accurate representation of the in soil root system.

227 **GLO-RIA: GLO-Roots Image Analysis** We developed a set of image analysis algo-
228 rithms that were well suited for the complex root systems that GLO-Roots is able to capture.
229 GLO-RIA (Growth and Luminescence Observatory Root Image Analysis) is an ImageJ plu-
230 gin divided in two modules. The first module (RootSystem) performs four different types of
231 analysis: i) a local analysis that detects all root particles in the image and computes their
232 position, length and direction; ii) the global analysis performs a root system level analysis
233 and computes the total visible surface, convex hull, width and depth; iii) the shape analysis
234 uses Elliptic Fourier Descriptors or pseudo-landmarks similarly to RootScape¹⁵ to perform
235 a shape analysis on the root system iv) the directionality analysis computes the mean direc-

tion of root particles in a root system (either on the full image or by a user-defined region of interest in the image). These four analysis methods are fully automated by default, but can be manually adjusted if needed. The second module of GLO-RIA (RootReporter) was specifically designed for the analysis of multi-layered images such as combinations of gene reporter, root structure and soil moisture. Shortly, the plugin works as follows: i) detection of the gene reporters and the structure reporters in their respective images; ii) if needed, a manual correction can be performed to correct the automated detection; iii) gene reporters are linked with the soil water content and the structure reporters, based on their proximity; iv) gene reporter intensity (either absolute or normalized using the structural reporter) is computed; v) all data are exported and saved to a RSML datafile¹⁶. Gene and structure reporters can be followed across different time and space points. Using an object oriented approach, great care has been taken to facilitate the user interactions on the different images to streamline the analysis process. Table 2 shows a list of root system features extracted using GLO-RIA. GLO-RIA does not currently have the ability to reconstruct the root architecture in itself (topological links between roots). This is a challenge for analyzing images captured by GLO-Roots since soil particles cause disruption of root segments.

Continuous imaging of root growth

The size of our rhizotrons enables undisturbed root system development (before roots reach the sides or the bottom of the rhizotron) for about 21-23 days for the Col-0 accession growing under long day conditions (Figure 2); however root traits such as directionality can be observed through later stages of plant development. See 35 DAS root system and directionality in Figure 2A-B. An example of a time series spanning 11 to 21 days after sowing (DAS) of Col-0 roots expressing *ProUBQ10:LUC2o* is shown in Fig 2A and [Video 1](#) with a color-coded time projection shown in Fig 2C. Directionality analysis (Fig 2B) shows a progressive change in root system angles from 0 ° (vertical) to 45 ° as lateral roots take over as the predominant root type. Figure 2D shows the evolution over time of several root traits that can be automatically captured by GLO-RIA (depth, width, area) and others that

²⁶³ were manually quantified (primary root growth rate or number of lateral roots per primary
²⁶⁴ root).

²⁶⁵ **Root system architecture of different *Arabidopsis* accessions.**

²⁶⁶ As a proof of concept to estimate the utility of our root imaging system to phenotype
²⁶⁷ adult root system traits, we transformed a small set of accessions (Bay-0, Col-0 and Sha)
²⁶⁸ with the *ProUBQ10:LUC2o* reporter and quantified RSA at 22 DAS (Fig 3A-C). GLO-RIA
²⁶⁹ analysis of these root systems identified several root traits that distinguish Col-0, Bay-0
²⁷⁰ and Sha. Directionality analysis revealed an abundance of steep-angle regions in the root
²⁷¹ system of Bay while Sha showed an abundance of shallow-angled regions and Col-0 was
²⁷² intermediate (Fig 3D). Bay-0 shows the deepest and narrowest root system leading to the
²⁷³ highest depth/width ratio while Sha has the widest root system (Fig 3E). Other root traits
²⁷⁴ such as root system area and the vertical center of mass also showed significant differences
²⁷⁵ (Figure 3-figure supplement 1B). Broad sense heritability values for depth (96.3), area (92.0),
²⁷⁶ depth/width (97.8), width (95.7) and vertical center of mass (95.0) were all higher than 90%.
²⁷⁷ To capture the richness of root architecture shape, we used GLO-RIA to extract pseudo-
²⁷⁸ landmarks describing the shape of the root system (see Materials and Methods for more
²⁷⁹ details) and performed PCA analysis. The first principal component captures differences
²⁸⁰ in the distribution of widths along the vertical axis and separates Col-0 and Sha from Bay-
²⁸¹ 0 root systems. (Fig 3F). Bay-0 shows an homogenous distribution of widths along the
²⁸² vertical axis while Sha and Col-0 are much wider at the top than bottom. PC2 seems to be
²⁸³ capturing a relationship between width at the top and total depth and separates Sha root
²⁸⁴ systems which are wide at the top and deep from Col-0 root systems which are wide but
²⁸⁵ not as deep as Sha. Shape information extracted from pseudo-landmarks can distinguish
²⁸⁶ the three different accession using PCA analysis (Fig 3G)

**287 Spectrally distinct luciferases enable gene expression patterns, characterization
288 of root system interactions and microbial colonization.**

289 We tested whether spectrally distinct luciferase reporters would enable additional informa-
290 tion besides root architecture to be captured from root systems. Luciferase reporters have
291 been commonly used to study gene expression and these resources can potentially be utilized
292 to study such regulatory events in soil-grown roots. We transformed *ProACT2:PpyRE8o*
293 into two well studied LUC reporter lines: the auxin response reporter line *ProDR5:LUC*¹⁷
294 (Figure A-B) and the Reactive Oxygen Species (ROS) response reporter *ProZAT12:LUC*¹⁸
295 (Figure 4C-D). We implemented in GLO-RIA an algorithm that semi-automatically iden-
296 tifies gene reporter signal and associates this object to the corresponding root structure
297 segment. A graphical representation of the results obtained with Root Reporter can be
298 observed in Figure 4E. Reporter intensity values along the first 5 mm of root tips can also
299 be observed in Figure 4-figure supplement 1. We then took advantage of our ability to
300 constitutively express two spectrally different luciferases and imaged the overlapping root
301 systems (one expressing *ProUBQ10:LUC2o* and the other *ProACT2:PPy RE8o*). While two
302 root systems were distinguishable using this system (Figure 4-figure supplement 2); mea-
303 surements of root system area did not reveal a significant effect on root growth when two
304 plants were grown in the same rhizotron, compared to one; however, further studies are
305 warranted (Figure 4-figure supplement 2).

306 The GLO-Roots system uses non-sterile growth conditions, which allows complex biotic
307 interactions that may affect responses to the environment. Bacteria themselves can be en-
308 gineered to express luminescent reporters through integration of the LUX operon, which
309 results in luminescence in the blue region of the spectrum and is thus compatible with
310 the plant-expressed luciferase isoforms we have tested. *Pseudomonas fluorescens* CH267¹⁹,
311 a natural *Arabidopsis* root commensal, was transformed with the bacterial LUX operon
312 and used to inoculate plants. Thirteen days after inoculation, we were able to observe
313 bacterial luminescence colocalizing with plant roots. *P. fluorescens* did not show an ob-
314 vious pattern of colonization at the root system scale level. As a proof-of-principle test

315 of the multi-dimensional capabilities of the GLO-Roots system we visualized both *LUC2o*
316 and *PPyRE8o* reporters in plants and the LUX reporter in bacteria in the same rhizotron
317 (Figure 4-figure supplement 3).

318 **Adaptive changes in root system architecture under water deprivation, phos-**
319 **phorus deficiency and light** To test the utility of the GLO-Roots system to understand
320 response of root systems to environmental stimuli we tested the effects of light and condi-
321 tions that mimic drought and nutritional deficiency. To examine the effects of light exposure
322 on the root architecture, the black shields, which normally protect the soil and roots from
323 light, were removed from the top half of the rhizotrons 10 DAS. Using directionality analysis
324 we detected a significant increase in the steepness of roots only in the light exposed region of
325 the rhizotron, while the lower shielded region showed no difference. (Fig 6-figure supplement
326 3A-B and Fig 6-figure supplement 4). Light can penetrate the top layers of soil²⁰ and it
327 has been proposed to have a role in directing root growth specially in dry soils²¹ through
328 the blue light receptor *phot1*. Root directionality was not significantly different between
329 light and dark-treated roots of the *phot1/2* double mutant suggesting that blue light per-
330 ception is necessary for this response^{21,22} (Fig 6-figure supplement 3B-lower panel). These
331 data highlight the strong effects of light on root system architecture²³, which GLO-Roots
332 rhizotrons are able to mitigate.

333 Plants grown in low-P soil showed a significant increase in the width-depth ratio of the root
334 system compared to plants grown in P-replete soil, as determined using the automated root
335 system area finder in GLO-RIA (Fig 6-figure supplement 2A-B). Plants under P deficiency
336 showed an increase in the ratio between root-shoot area (Fig 6-figure supplement 2C) and
337 higher investment of resources in the development of the root system at the expense of shoot
338 growth (Fig 6-figure supplement 2D). Root systems of control and P-deficient plants showed
339 no significant differences in directionality at 22 DAS but at 27 DAS, roots were more hori-
340 zontally oriented in P-deficient plants (Fig 6-figure supplement 2E). The observed changes in
341 root architecture are consistent with root system ideotypes that improve phosphorus uptake
342 efficiency.

343 GLO-Roots is especially well suited for studying water-deficit (WD) responses. First, shoots
344 are exposed to the atmosphere and vapor pressure deficit (VPD) is maintained at levels that
345 allow for transpiration of water from the shoot. Second, soil in rhizotrons is exposed to air
346 at the top and dries basipetally (from the top-down); drying soil increases the volume
347 occupied by air and reduces contact of root with liquid water, all of which are similar to
348 changes in soil expected in the field during WD. Finally, as peat-based soil dries, its optical
349 properties change, allowing moisture content to be approximated from bright-field images.
350 We took advantage of the change in gray-scale pixel intensity to construct a calibration
351 curve (Figure 5-figure supplement 1) that quantitatively relates gray-scale pixel intensity to
352 moisture content (Fig 5A); water content can be color coded in images with appropriate
353 look up tables (Fig 5B). Soil color was not affected by the presence or absence of roots
354 (Figure 5-figure supplement 2). Using this approach, water content in a rhizotron can be
355 mapped and visualized in 2D (Fig 5C-D). In the example shown, we can observe that a 22
356 DAS Bay-0 plant depleted soil-moisture content locally around the the root system (Figure
357 5E).

358 We performed several trials to simulate WD in our growth system. Plants were germinated,
359 grown under control conditions then transferred to 29°C and standing water removed from
360 the container holding the rhizotrons starting at 9 DAS or 13 DAS. Elevated temperature
361 combined with water deficit is a common stress that modern crops varieties are poorly
362 adapted to, thus highlighting the importance of examining this combined treatment^{24,25}.
363 Plants were maintained in this WD regime until 22 DAS when luciferin solution was added
364 and the plants imaged. At 13 DAS, lateral roots near the soil surface are already emerged
365 ([Video 1](#), Figure 2A) and 9 days of subsequent WD treatment caused lateral roots to show an
366 increase in gravitropism leading to the development of a root system that were deeper and
367 more vertically oriented (Fig 6A). Roots of Bay-0 plants showed similar responses, though
368 the extent of change was less pronounced since Bay-0 roots are normally more vertically
369 oriented (Fig 6B). Plants transferred at 9 DAS and grown for 13 days under WD showed
370 less lateral root development in the top layer of soil (Fig 6E). At this time point, lateral roots
371 start to emerge ([Video 1](#)) and early drought may lead to growth quiescence or senescence.

³⁷² Careful examination of roots in these regions showed evidence of small lateral root primordia
³⁷³ populating the primary root (Figure 6F). After 24 h of re-watering (Figure 6G) these lateral
³⁷⁴ root primordia reinitiated growth (Figure 6H).

³⁷⁵ Time-lapse imaging of the water deficit response showed that changes in root growth direc-
³⁷⁶ tion occurred ahead of the dry soil front [Video 2](#). Using GLO-RIA we were able correlate
³⁷⁷ local water moisture contents with the orientation of root segments. With this approach we
³⁷⁸ observed that root segments in dryer areas of rhizotron grew at steeper root angles (Figure
³⁷⁹ 7) than roots in WW regions, though lateral root angle in wetter regions was also affected.
³⁸⁰ These data suggest that both local and systemic signaling is likely involved in redirecting
³⁸¹ lateral roots deeper during the simulated drought treatments tested here.

³⁸² We also grew plants under WD at control temperatures or under WW conditions at elevated
³⁸³ temperature to test the effects of these individual stresses on root architecture. We observed
³⁸⁴ that both conditions were sufficient to induce a change in root directionality indicating that
³⁸⁵ the plant uses similar mechanisms to avoid heat and water-deficit associated stresses (Figure
³⁸⁶ 6-figure supplement 1). We next asked which regulatory pathways controlled the observed
³⁸⁷ changes in lateral root directionality during simulated drought. Hydrotropism is a known
³⁸⁸ environmental response that directs root growth towards wet regions of soil. MIZ1 is an
³⁸⁹ essential regulator of hydrotropism; however *miz1* mutants had no significant effect on water
³⁹⁰ deficit-induced changes in root directionality, compared to wild type (Fig 6C), indicating
³⁹¹ that this response was distinct from hydrotropism. Auxin is an important mediator of
³⁹² gravitropism and auxin treatment causes lateral roots to grow more vertically⁷. Consistent
³⁹³ with this role for auxin, mutant plants with loss of function in the auxin receptor TIR1, did
³⁹⁴ not show changes in the root system directionality between WW and WD conditions (Fig
³⁹⁵ 6D).

³⁹⁶ **GLO-Roots for Brachypodium and Tomato.**

³⁹⁷ To examine the general applicability of the GLO-Roots system for other species, we intro-
³⁹⁸ duced LUC2o-expressing reporters into the model grass *Brachypodium distachyon* and the

³⁹⁹ crop plant *Lycopersicon esculentum* (tomato). Brachypodium is well suited to the GLO-Root
⁴⁰⁰ system because, like Arabidopsis, its small size allows mature root systems to be studied in
⁴⁰¹ relatively small soil volumes^{26,27}. *LUC2o* driven by the *ZmUb1* promoter was introduced into
⁴⁰² Brachypodium using the pANIC vector²⁸. Brachypodium roots showed a distinct architec-
⁴⁰³ ture from Arabidopsis marked by prolific development of secondary and tertiary lateral roots
⁴⁰⁴ (Fig 8A). This is consistent with other studies that show that Brachypodium has a typical
⁴⁰⁵ grass root system²⁷. Comparison of root system development in rhizotrons with gel-based
⁴⁰⁶ media showed that root growth is higher in soil than in plates (Figure 8-figure supplement
⁴⁰⁷ 1). Previous work has suggested that auxin levels in Brachypodium roots is sub-optimal for
⁴⁰⁸ growth²⁹. Pacheco-Villalobos and colleagues suggest that, in Brachypodium, and contrary
⁴⁰⁹ to what happens in Arabidopsis, ethylene represses *YUCCA* reducing the synthesis of auxin.
⁴¹⁰ The reduced growth that we observe in plates and the high levels of ethylene that build up
⁴¹¹ in sealed plates³⁰ would support this mechanism.

⁴¹² Tomato plants were transformed with *Pro35S:PPyRE8o* and *ProeDR5rev:LUC2* reporters.
⁴¹³ The plants showed more rapid growth than Arabidopsis or Brachypodium and required
⁴¹⁴ fertilizer to prevent obvious signs of stress (reduced growth, anthocyanin accumulation).
⁴¹⁵ Root systems were imaged from 17 DAS plants. Roots showed presumptive lateral root
⁴¹⁶ primordia marked by DR5-expression (Fig 8C-D). These results show that the GLO-Roots
⁴¹⁷ method can be applied to study root systems of plants and will likely be useful for studying
⁴¹⁸ root systems of other small to medium sized model plants and for early stages of larger crop
⁴¹⁹ plants.

⁴²⁰ **Discussion**

⁴²¹ **GLO-Roots enables a multi-dimensional understanding of root biology**

⁴²² Recent studies of root systems has emphasized structural attributes as important contrib-
⁴²³ utors of root system function. Indeed, studies examining the role of genetic variants in
⁴²⁴ tolerating abiotic stress have demonstrated the importance of such characteristics⁸. Roots,

425 however, are highly diverse in the biology they perform and a multi-dimensional understand-
426 ing of root systems, which incorporates differences in signaling, metabolism and microbial
427 association as well as structure, may provide a clearer understanding of the degree to which
428 sub-functionalization of the root system plays a role in important processes such as acclima-
429 tion and efficient resource acquisition.

430 We have developed tools in GLO-Roots that allow for tracking multiple aspects of soil
431 physicochemical properties and root biology simultaneously. Using GLO-Roots, we are able
432 to map in 2D coordinates soil physical properties such soil moisture together with root ar-
433 chitecture traits such as directionality, growth rates and gene expression levels. All this
434 information is aggregated in layers for each x, y coordinate. Using GLO-RIA we integrate
435 this multilayer information, leveraging our ability to simultaneously and seamlessly inves-
436 tigate root responses to environmental stimuli such as soil moisture content. Luciferase
437 isoforms that emit light at different wavelengths allow for constitutive and regulated pro-
438 moters to be studied together. Introduction of luciferase reporters into microbes provides
439 an additional layer of information that provides a readout on the association between or-
440 ganisms and how this might be affected by environmental conditions. The flexibility of the
441 GLO-Roots system may enable additional dimensionality to our understanding of root biol-
442 ogy. Other physical properties such as CO₂ or pH mapping in rhizotrons have already been
443 enabled by using planar optodes³¹. It may be possible to engineer LUX-based reporters
444 in microbes that are responsive to extracellular metabolites, creating microbial biosensors,
445 and integration of such tools may enable root-exudation and nutrition to be analyzed in
446 soil. Split-Luciferase reporters have been engineered that allow bi-molecular interactions to
447 be studied. Finally, molecular sensors analogous to FRET sensors, termed BRET-sensors³²,
448 may allow metabolite tracking dynamically through the root system. With additional inno-
449 vation in the development of luciferase reporters, the GLO-Roots systems will likely expand
450 the repertoire of biological processes that can be studied over an expanded range of devel-
451 opmental time points and environmental conditions.

**452 Enhanced root growth and gravitropism may constitute an avoidance mechanism
453 used during water deficit stress**

454 It has been proposed that plants with steep root systems will be better able to tap into deep
455 water resources and thus perform better under water deprivation. For example in rice, the
456 IR64 paddy cultivar shows shallow root systems in upland fields whereas Kinandang Patong,
457 an upland cultivar, is deeper rooting⁸. Plants maintain a number of regulatory pathways that
458 mediate changes in physiology during WD. Enhanced growth of root systems has been well
459 characterized in field-grown plants; however this has not been recapitulated in studies of gel-
460 grown Arabidopsis plants. Thus, it has been unclear whether Arabidopsis simply responds
461 to WD differently. Our results here show that Arabidopsis does indeed maintain a classical
462 WD response that expands the root system and directs growth downward. Interestingly,
463 under our stress regime, we did not observe a significant decrease in the relative water
464 content of shoot tissues (Figure 6-figure supplement 5), suggesting that the changes in root
465 architecture were sufficient to provide access to deep water and prevent dehydration. Such
466 changes in root growth are likely regulated through systemic and local signaling that involve
467 auxin signaling but acts independently of known pathways that control moisture-directed
468 root growth.

469 Perspectives and Conclusions

470 Understanding plant biology requires a sophisticated understanding of how environmental
471 stimuli affect the form and function of plants as well as an understanding of how physiological
472 context informs such responses. Environmental conditions are at least as complex as the
473 plants they affect. Plant roots are exposed to a variety of environmental signals that change
474 in time and space at very different scales that are integrated at the whole plant system. It is
475 an important challenge in biology to develop methods of growing and studying plants that
476 present such stimuli in a manner that the plant is likely to encounter in nature. After all, the
477 plants we study have evolved to survive through mechanisms that have been selected, over
478 evolutionary time, in nature. It will be interesting for future studies to determine how other

479 environmental stimuli affect root growth using GLO-Roots and whether these responses
480 differ between accessions of Arabidopsis. Identification of the genetic loci responsible for
481 phenotypic variation in adult root phenotypes may identify the molecular basis for adaptive
482 variation that exists in this species and potentially identify loci that are useful for breeding
483 efforts needed for the next green revolution.

484 **Materials and methods**

485 **Growth system**

486 **Rhizotrons and growth system fabrication.** Rhizotrons are composed of two sheets of
487 1/8" abrasion resistant polycarbonate plastic (Makrolon AR (R)) cut to size using a water
488 jet (AquaJet LLC, Salem, OR), two acrylic spacers cut using a laser (Stanford Product
489 Realization Lab), two rubber U-channels cut to strips 30 cm long ([McMaster Carr part](#)
490 [# 8507K33](#)) and two sheets of black 0.030" thick polypropylene sheets ([McMaster Carr](#)
491 [part # 1451T21](#)) cut with a straight-edge razor blade. Rhizotron designs were drafted in
492 Adobe Illustrator (Adobe, San José, CA). The blueprints of all the parts are provided in
493 Supplement 1. The top edge of each polycarbonate sheet was painted with black 270 Stiletto
494 nail polish (Revlon, New York, NY).

495 **Boxes and holders.** Rhizotrons are held vertical during plant growth in a custom rack sys-
496 tem composed of two sheets of 1/4" black acrylic plastic cut with slots for eleven rhizotrons
497 using a laser, four 3/8" PVC rods ([McMaster Carr part # 98871a041](#)) secured with PVC
498 nuts ([McMaster Carr part # 94806a031](#)) to hold the acrylic sheets horizontal. The rack is
499 placed inside a 12" x 12" x 12" black polyethylene tank ([Plastic Mart part # R121212A](#)).

500 **Rhizotron preparation** The procedure to construct a rhizotron with soil is as follows:
501 Two pieces of polycarbonate plastic are laid flat on a table with the spacers inserted. Using
502 an electric paint gun, a fine mist of water is applied to the bare polycarbonate sheets. Then,
503 using a 2 mm sieve (US Standard Sieve Series N° 10) a fine layer of PRO-MIX(r) PGX soil
504 (Premier Tech, Canada) is applied. Excess soil is discarded by gently tapping the plastic

505 against the table in a vertical position. Water is sprayed again onto the soil, then a second
506 layer of Pro-MIX is applied as before. For P deficiency experiments soil supplemented with
507 1 ml of 100 µM P-Alumina (control) and 0-P-Alumina (P deficient) was used. To prevent
508 the soil from falling out of the bottom opening, a 3 x 6 cm piece of nylon mesh is rolled into
509 a 1 cm wide tube and placed at the bottom side of the rhizotron. The spacers are removed
510 and replaced by clean spacers. The two faces of the rhizotron are carefully joined together
511 and two rubber U-channels slipped on to clamp all pieces together. Assembled rhizotrons
512 are placed into the rack inside the boxes and 500 mL of water is added to the box.

513 **Plant growth** *Arabidopsis thaliana* seeds were stratified for 2 d at 4 °C in Eppendorf tubes
514 with distilled water. Seeds were suspended in 0.1 % agar and 5 to 10 were sown using
515 a transfer pipette in the rhizotron. A transparent acrylic sheet was mounted on top of
516 the box and sealed with tape to ensure high humidity conditions that enable *Arabidopsis*
517 germination. Three days after sowing, the cover was unsealed to decrease humidity and
518 allow the seedlings to acclimate to a dryer environment. From 3 days after sowing (DAS)
519 to the time the first true leaves emerged, it was critical to ensure that the top part of the
520 rhizotron remained humid for proper germination of the plants. Between three and five DAS
521 the rhizotrons were thinned leaving only the number plants required for that experiment,
522 typically one, except for experiments examining root-root interactions. Unless otherwise
523 stated, all the experiments presented here, treatments were started 10 DAS. Plants were
524 grown under long day conditions (16 h light / 8 h dark) using 20–22 °C (day/night) and
525 150 µE m⁻¹ s⁻¹. Two types of growth environments were used for experiments. A walk-in
526 growth chamber with fluorescent lightning and a growth cabinet with white LED lights.
527 Relative water content measurements were done as previously described³³

528 **qRT-PCR analysis.**

529 Seeds were surface sterilized as described before² and grown in rhizotrons, 100 cm³ pots, or
530 on two types of 1% agar (Duchefa) media containing either 1x MS nutrients (Caisson) and 1%
531 Sucrose, (termed ms media) or 1/4x MS nutrients only (termed ms25 media). Both media were

532 buffered using 0.5 g/L MES and pH was adjusted to 5.7 with KOH. All plants were grown
533 together in a growth cabinet with LED lights under long day conditions (16h day/8h night).
534 Root and shoot tissue was collected separately from individual plants at the end of the day
535 (1 hour before the lights shut off) and at the end of the night (1 hour before lights came on).
536 Three biological replicates were collected for each condition. RNA was extracted using the
537 Plant RNA MiniPrepTM kit (ZYMO Research) according to manufacturer's instructions
538 with on-column DNase treatment (Qiagen). cDNA was made using the iScript Advanced
539 cDNA Synthesis for RT-qPCR kit (Bio-Rad) from 200 ng of total RNA. qRT-PCR was
540 performed using a Fluidigm BioMarkTM 96.96 Dynamic Array IFC with the EvaGreen®
541 (Bio-Rad) fluorescence probe according to the Fluidigm Advanced Development Protocol
542 number 37. For the analysis, all the reactions with no amplification ($C_t = 999$) were set
543 to the maximal C_t for that assay type. The two technical replicates were then averaged
544 and dC_t values calculated using AT3G07480, AT4G37830, At1g13320 and At1g13440 as
545 reference internal controls. PCA plots were generated with Devium Web³⁴ using dC_t values.
546 Primers used are listed in file Supplement 8.

547 **Biological components**

548 **Codon optimization of luciferases.** The following luciferases that emit light at different
549 wavelengths were codon optimized for Arabidopsis (Genscript, Piscataway, NJ): LUC2: a
550 yellow improved version (Promega, Madison, WI) of the original *Photinus pyralis* (firefly)
551 LUC.

- 552 • Ppy RE8: a red variant³⁵ of the *P. pyralis* thermostable variant Ppy RE-TS³⁶.
- 553 • CBG99: a green variant (Promega, Madison, WI) from yellow click beetle (*Pyrophorus*
554 *plagiophthalmus*) luciferases.
- 555 • CBR: a red variant (Promega, Madison, WI) from yellow click beetle.

556 **Non-optimized luciferases.** We also used the following non-optimized luciferases:

- 557 • nanoLUC: a blue luciferase isolated from a deep sea shrimp¹⁴.
- 558 • venusLUC2: a venus-LUC2 fusion reported to show higher luminescence output than
559 LUC2¹².
- 560 • A transposon containing the bacterial luciferase-containing LUX operon was inte-
561 grated into the *Pseudomonas fluorescens* CH267¹⁹ genome by conjugation with *E.*
562 *coli* *SM10 pir* containing pUT-EM7-LUX³⁷ and used to track root microbe coloniza-
563 tion. For inoculation 9 DAS plants were inoculated with 2 mL of an overnight bacterial
564 culture resuspended in 10 mM MgSO~4 and diluted to 0.01 OD.

565 **Generation of single-reporter transgenic plants.** We generated transcriptional fu-
566 sions of all luciferases to constitutive promoters to examine the activity level and emission
567 spectrum of each isoform. The *attL1-attL2* entry clones containing plant-codon optimized
568 coding sequence of *LUC2*, *PpyRe8*, *CBG99* and *CBR* were synthesized by Genscript. A
569 DNA fragment including the *UBQ10* promoter region and first intron was amplified from
570 Col-0 genomic DNA with primers incorporating the attB1, attB4 combination sites at the 5'
571 and 3' respectively. The PCR product was then introduced into pDONR™ P4-P1R (Invitro-
572 gen) through a classic Gateway BP-reaction. The resulting plasmid, the *attL1-attL2* entry
573 clones with luciferase sequences, an empty *attR2-attL3** entry clone and the destination
574 vector dpGreenmCherry² were used to construct *ProUBQ10:LUC2o*, *ProUBQ10:PpyRE8o*,
575 *ProUBQ10:CBG99o* and *ProUBQ10:CBRo* through Gateway LR reactions. The destination
576 vector *dpGreenmCherry* contains a plasma membrane-localized mCherry coding sequence
577 driven by the 35S promoter and is used as a selectable marker of transformation at the
578 mature seed stage². We used Golden Gate cloning and the destination vectors that we had
579 generated before¹³ for the following fusions: *ProUBQ10:nanoLUC2*, *ProUBQ10:venusLUC*,
580 *ProACT2:PpyRE8o*. Briefly, the different components of each construct were PCR ampli-
581 fied with complementary BsaI or SapI cutting sites, mixed with the destination vector in
582 a single tube, digested with either BsaI or SapI, ligated with T4 DNA ligase, then trans-
583 formed into *E. coli* Top10 cells and plated on LB antibiotic plates containing X-gal as pre-

584 viously described¹³. Junction sites were confirmed by sequencing. We used pSE7 (Addgene
585 ID #: pGoldenGate-SE7: 47676) as the destination vector of the *ProUBQ10:nanoLUC2*,
586 *ProUBQ10:venusLUC* constructs and pMYC2 (Addgene ID #: pGoldenGate-MCY2: 47679)
587 as the destination vector for *ProACT2:PpyRE8o*. Maps of all the vectors can be found in
588 Supplement 8. *ProUBQ10:LUC2o* was transformed into Col-0, Bay and Sha accessions, the
589 *tir1-1*³⁸ mutant and the *mizf*³⁹ T-DNA insertion line (SALK_126928).

590 **Brachypodium distachyon** The Arabidopsis plant-codon optimized Luciferase gene,
591 *LUC2o*, was inserted into the monocot vector pANIC10 via Gateway cloning²⁸. *Brachy-*
592 *podium distachyon* plants were transformed using the method of Vogel and Hill⁴⁰.

593 **Tomato** The transcriptional fusion *ProeDR5:LUC2* was generated by cloning the
594 *ProeDR5:LUC2* DNA fragment into the pBIB expression vector via restriction sites SalI
595 and Acc65I. The eDR5 promoter is an enhanced version of DR5 containing 13 repeats of
596 the 11-nucleotide core DR5 element⁴¹ and the pBIB expression vector contains an NPTII
597 resistance gene under the control of the NOS promoter for use as a selectable marker during
598 transformation. All tomato transformations were performed by the Ralph M. Parsons
599 Foundation Plant Transformation Facility (University of California, Davis).

600 **Generation of dual-reporter plants.** To generate dual-reporter plants expressing lu-
601 ciferase isoforms that emit light with divergent emission spectra we used *ProACT2:PpyRE8o*
602 as the root structural marker and ZAT12:LUC¹⁸ and DR5:LUC+¹⁷ lines that were trans-
603 formed with the *ProACT2:PpyRE8o* construct. All constructs were transformed using a
604 modified floral dip method as described in².

605 To make the dual color tomato plants, the *Pro35S:PpyRE8o* transcriptional fusion was
606 generated by putting the plant-codon optimized coding sequence described above into the
607 pMDC32 expression vector through a Gateway LR reaction. The pMDC32 vector con-
608 tains a hygromycin resistance gene under the control of the 35S promoter for use as a se-
609 lectable marker during transformation. This construct was transformed into the transgenic

610 *ProeDR5:LUC2* tomato line.

611 **In vivo emission spectra of plants constitutively expressing luciferase isoforms.**

612 To generate *in vivo* emission spectra of all constitutively expressed luciferases, seeds were
613 sterilized and sown on MS plates as described before². After 8 days, seedlings were treated
614 with a 100 µM luciferin solution, incubated at room temperature for 3 hours and imaged
615 using an IVIS Spectrum imaging system (Perkin Elmer, Waltham , MA) using 20 nm band-
616 pass emission filters at the following wavelengths (in nm: 490-510, 510-530, 530-550, 550-570,
617 570-590, 590-610, 610-630, 630-650, 650-670, 670-690, 690-710). Raw images were analyzed
618 using Fiji and *in vivo* emission spectra were constructed. The full emission spectra of LUX
619 and nanoLUC could not be constructed since the maximum of these two luciferases is below
620 the lower band pass filter that were available.

621 **Imaging system** We designed a custom imaging system (GLO1, Growth and Lumines-
622 cence Observatory 1) optimized for imaging dual-reporter luciferase expression in our custom
623 rhizotrons. The design was a joint effort with Bioimaging Solutions (San Diego, CA) who
624 also built the system and wrote the acquisition software that drives all the mechanical parts
625 of the system. The system is composed by two 2048 x 2048 PIXIS-XB cameras (Princeton
626 Instruments, Trenton, NJ) mounted on top of each other to capture two fields of view en-
627 compassing approximately two 15 x 15 cm areas corresponding to the top or bottom of the
628 rhizotron. The cameras are fitted with a Carl-Zeiss macro lens. A filter wheel with space
629 for four, 76.2 mm filters is positioned in front of the cameras and controlled by a stepper
630 motor allowing for automated changing of the filter wheel position. We used two -542/50
631 and 450/70- custom cut Brightline(R) band-pass filters (Semrock, Rochester, NY). In sin-
632 gle color imaging mode, the filter wheel is operated without filters. Positioned in front of
633 the filter wheel is a removable rhizotron holder mounted on a stepper motor. This stepper
634 motor is also controlled by the GLO-1 software allowing automatic acquisition of images
635 from both sides of the rhizotron sequentially. The whole imaging system is enclosed in a
636 light-tight black box with a door that allows loading and un-loading of rhizotrons.

637 **Plant Imaging** Around 50 mL of 300 μ M D-luciferin (Biosynth, Itasca, IL) was added to
638 soil at the top of the rhizotron. In general 5 min exposures were taken per rhizotron, per
639 side, per channel. For daily imaging experiments, plants were imaged at dawn (+/- 1 hr)
640 to reduce possible effects on diurnal rhythms of keeping plants in the dark during imaging.
641 Shoot images were taken using a Nikon D3100 camera.

642 **Image Preparation** Four individual images are collected: top front, bottom front, top
643 back and bottom back. Using an automated [ImageJ macro](#), a composite image is generated
644 as follows: 1) To correct for differences in background values between the two cameras the
645 mean background value of each image is subtracted from 200; 2) images are rotated and
646 translated to control for small misalignments between the two cameras; 3) the top and
647 bottom images of each side are merged; 4) the back image is flipped horizontally; 5) the
648 front and back images are combined using the maximum values. When dual color images are
649 acquired this operation is repeated for each channel. The final images produced are 16-bit
650 depth and 4096 x 2048 pixels. The scale of the images is 138.6 pixels per cm. Considering
651 that an Arabidopsis root is 100 μ m this results in 1.39 pixels across an Arabidopsis root.

652 **GLO-RIA imageJ plug-in** GLO-RIA uses a combination of existing tools to extract
653 relevant root architecture features. Directionality is acquired using the [directionality plugin](#)
654 from ImageJ. After the number of direction bins (we usually use bins of 2 $^{\circ}$) is defined by the
655 user, a 5x5 sobel operator is used to derive the local gradient orientation. This orientation
656 is then used to build a distribution of directions by assigning the square of the orientation
657 into the appropriate bin. Instead of representing the total counts at each orientation a
658 relative value is calculated by dividing the individual values at each bin by the total sum
659 of the histogram (and multiplying by 100). Similar algorithms have been used to quantify
660 dynamic changes in the plant cytoskeleton⁴².
661 The Elliptic Fourier Descriptors are acquired using the [Fourier Shape Analysis plugin](#) on
662 convex hull shape of the root system. Elliptic Fourier Descriptors have been used in numer-
663 ous studies to analyse variations in shapes, notably in leaves (e.g⁴³) The shape analysis is

664 inspired by RootScape¹⁵. Due to the absence of fixed, recognisable structures in root system
665 (that are required for the position of true landmarks), pseudo-landmarks are automatically
666 extracted from the root systems. Shortly, the image is divided vertically at equidistant posi-
667 tions (with the number defined by the user) and for each of the image stripes, the minimum
668 and maximum x coordinates are computed. The shape analysis is therefore able to discrim-
669 inate root system with different vertical root distributions or global root system orientation
670 (e.g. chemotropism) . The code source for the plugin, manual and sample images can be
671 found in the [github repository](#) of the project.

672 Statistical analysis was performed in R⁴⁵. The tidyR⁴⁶, dplyr⁴⁶, gridExtra⁴⁷, shapes⁴⁸,
673 geomorph⁴⁹, ggplot2⁵⁰ and cowplot⁵¹ packages were used for data preparation, analysis
674 and plotting. Final figure preparation was done in [Inkscape](#).

675 **Data availability** All the scripts and original data used to analyze and produce the
676 images can be accessed in the Github repository of the project: github.com/rr-lab/GLO-Roots. Raw files of all the images used in the paper are available in [Dryad](#).

678 Acknowledgements

679 Work in the lab of JRD was funded by the Carnegie Institution for Science Endowment
680 and grants from the National Science Foundation (MCB-115795) and Department of En-
681 ergy, Biological and Environmental Research program (DE-SC0008769). RRA was sup-
682 ported by a Carnegie Postdoc Fellowship and currently by Conacyt Ciencia Básica Joven
683 Investigador grant number (CB-2014-01-238101). GL was supported by the Belgian Fonds
684 de la Recherche Scientifique. JM was funded by the National Science Foundation (IOS-
685 0820854). CH is funded by MGH Toteston & Fund for Medical Discovery Fellowship grant
686 2014A051303 and NIH R37 grant GM48707 and NSF grant MCB-0519898 awarded to Fred-
687 erick Ausubel, and previously by the Gordon and Betty Moore Foundation through Grant
688 GBMF 2550.01 from the Life Sciences Research Foundation. JV was funded by the Office
689 of Biological and Environmental Research, Office of Science, US Department of Energy, in-

690 teragency agreements DE-SC0001526 and DE-AI02-07ER64452. We thank Robert Mittler
691 and Philip Benfey for providing seeds of ZAT12:LUC and DR5:LUC+ respectively. We also
692 thank Neil Robbins and members of the Dinneny lab for critical review of the manuscript
693 and suggestions during the development of the project. We greatly appreciate Tim Doyle at
694 the Stanford Small Animal Imaging Facility for providing's advice in using and help with
695 luciferase-based imaging approaches.

696 **Competing interests**

697 We do not have any competing interests that we are aware of.

698 **Tables**

699 **Table 1:** Luciferases used in this study.

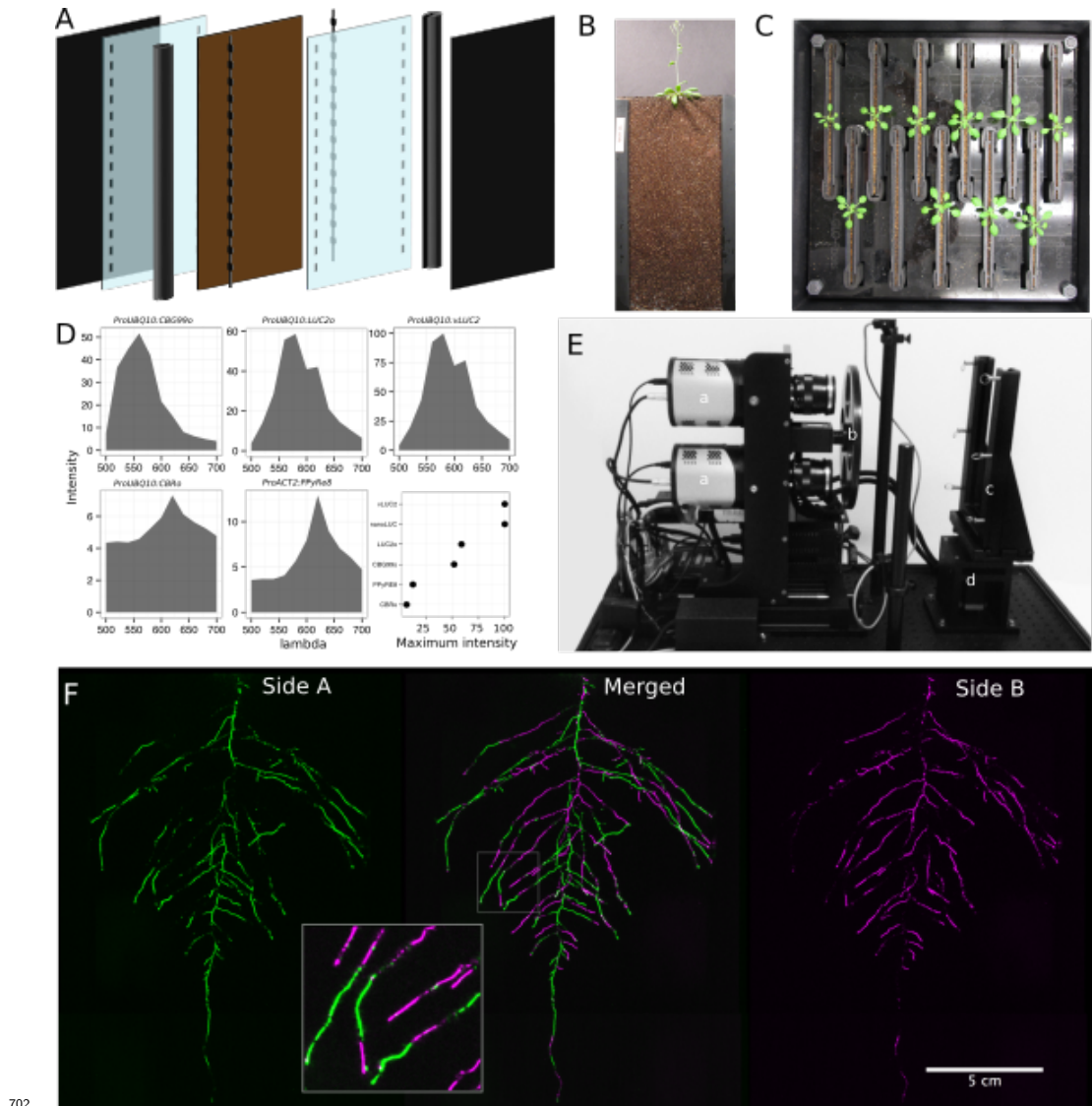
| Luciferase | Origin | maximum wavelength | Substrate |
|------------|-----------------|--------------------|--|
| Ppy RE8 | firefly | 618 | D-luciferin |
| CBGRed | click beetle | 615 | D-luciferin |
| venus-LUC2 | FP + firefly | 580 | D-luciferin |
| LUC(+) | firefly | 578 | D-luciferin |
| CBG99 | click beetle | 537 | D-luciferin |
| lux operon | A. fischeri | 490 | biosynthesis pathway encoded within operon |
| nanoLUC | Deep sea shrimp | 470 | furimazine |

700 **Table 2:** list of root system features extracted using GLO-RIA.

| variable | unit |
|-------------------------|------|
| projected area | cm^2 |
| number of visible roots | - |
| depth | cm |

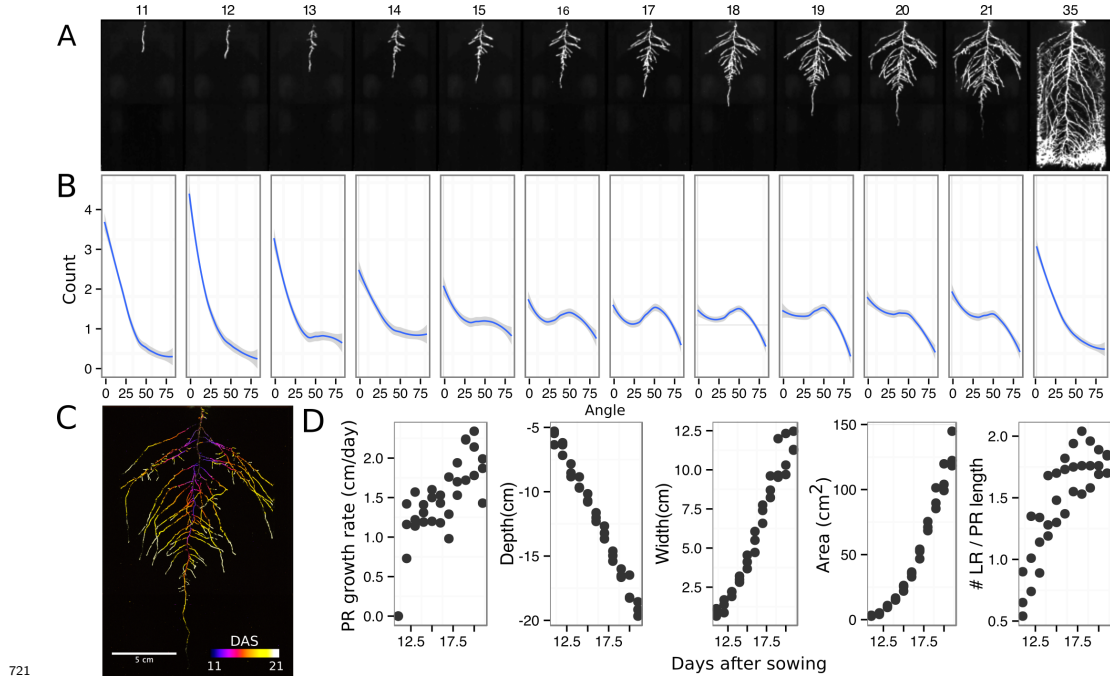
| variable | unit |
|-------------------------------|-----------------|
| width | cm |
| convex hull area | cm ² |
| width | cm |
| feret | cm |
| feret angle | ° |
| circularity | - |
| roundness | - |
| solidity | - |
| center of mass | cm |
| Directionality | ° |
| Euclidean Fourier Descriptors | - |
| Pseudo landmarks | - |

701 **Figures**



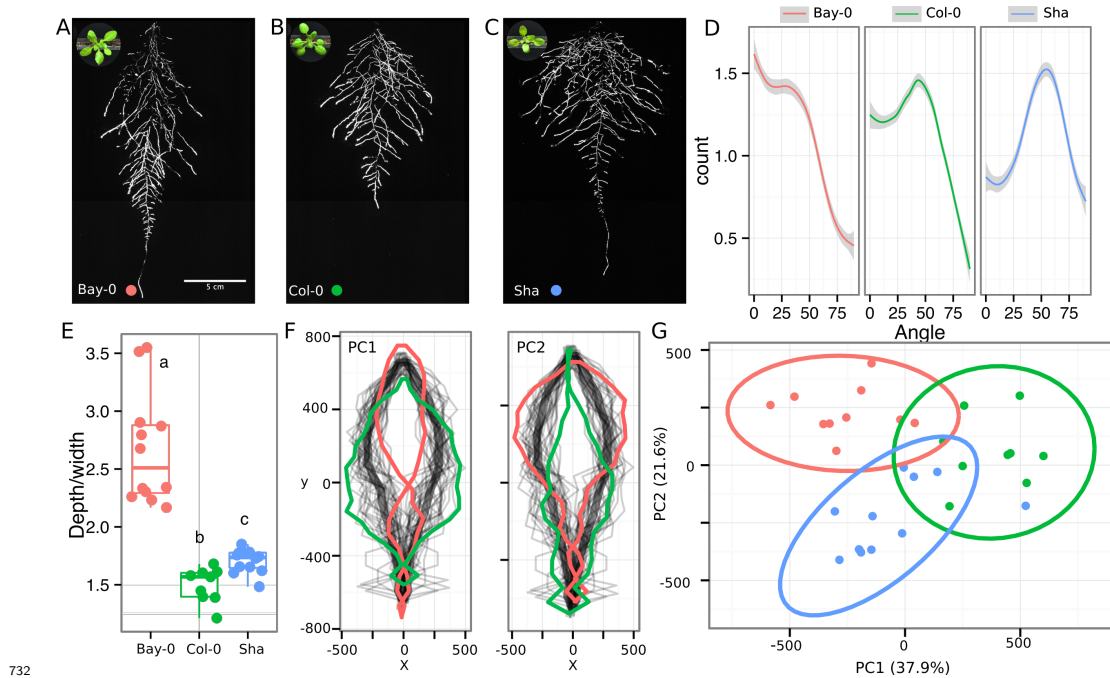
703 **Figure 1. GLO-Roots growth and imaging systems** A) 3D representation of the
 704 different physical components of the rhizotron: plastic covers, polycarbonate sheets,
 705 spacers and rubber U-channels. Blueprints are provided in Supplementary material 1. In brown,
 706 soil layer. B) Thirty five day-old plant in rhizotron with black covers removed. C) Top view
 707 of holding box with eleven rhizotrons. D)In vivo emission spectra of different luciferases
 708 used in this study. Transgenic homozygous lines expressing the indicated transgenes were

709 grown on agar media for 8 days. Luciferin (300 μ M) was sprayed on the seedlings and
 710 plates were kept in the dark and then imaged for 2 s at wavelengths ranging from 500
 711 to 700 nm. Five intensity values were taken from different parts of the roots of different
 712 seedlings and averaged. Relative maximum intensity values are indicated in the lower right
 713 graph. E) GLO 1 imaging system. The system is composed by two back illuminated CCD
 714 cameras (a) cooled down to -55 °C. A filter wheel (b) allows for spectral separation of the
 715 different luciferases. On the right, a rhizotron holder (c) is used to position the rhizotrons
 716 in front of the cameras. A stepper motor (d) rotates the rhizotron 180° to image both
 717 sides. F) A 21 DAS plant expressing *ProUBQ10:LUC2o* was imaged on each of two sides
 718 of the rhizotron; luminescence signal is colorized in green or magenta to indicate side. In
 719 the middle of the panel, a combined image of the two sides is shown. The inset shows a
 720 magnified part of the root system. FW: fresh weight, PR: Primary root.

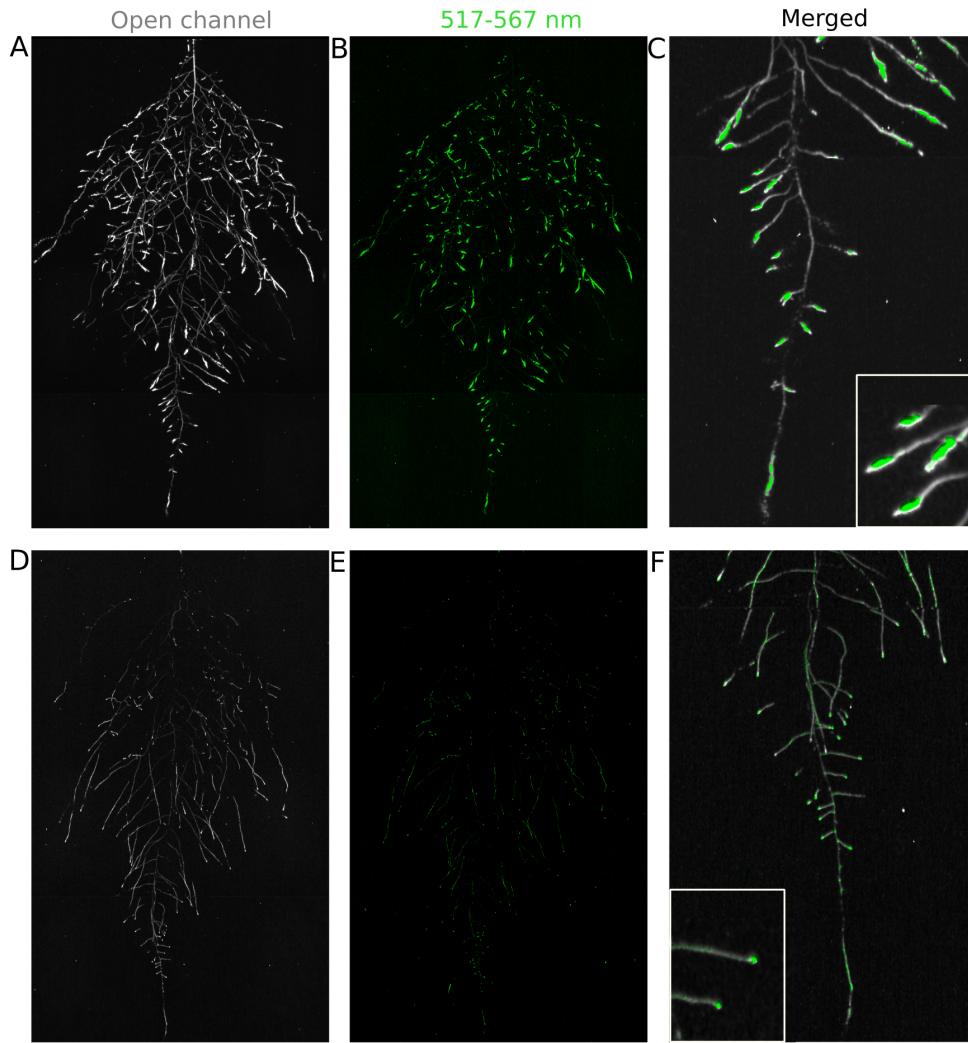


722 **Figure 2. Time-lapse imaging of root systems and quantification using GLO-**
 723 **RIA.** A) Typical daily time-lapse image series from 11 to 35 DAS of a *ProUBQ10:LUC2o*
 724 Col-0 plant. B) Directionality of the root system of plants in panel A calculated using the
 725 directionality plugin implemented in GLO-RIA. C) Color coded projection of root growth

726 using the images in panel A. D) Primary root growth rate, depth, width, root system area
 727 are automatically calculated from the convex hull, which is semi-automatically determined
 728 with GLO-RIA. Lateral root number and number of lateral roots divided by the primary
 729 root length were quantified manually. A Local Polynomial Regression Fitting with 95%
 730 confidence interval (grey) was used to represent the directionality distribution curve. (0° is
 731 the direction of the gravity vector).



743 with 95% confidence interval (grey) was used to represent the directionality distribution
744 curve. 0° is the direction of the gravity vector. Wilcoxon test analysis with $p < 0.01$ was
745 used to test significant differences between the different accession ($n = 9-12$ plants).

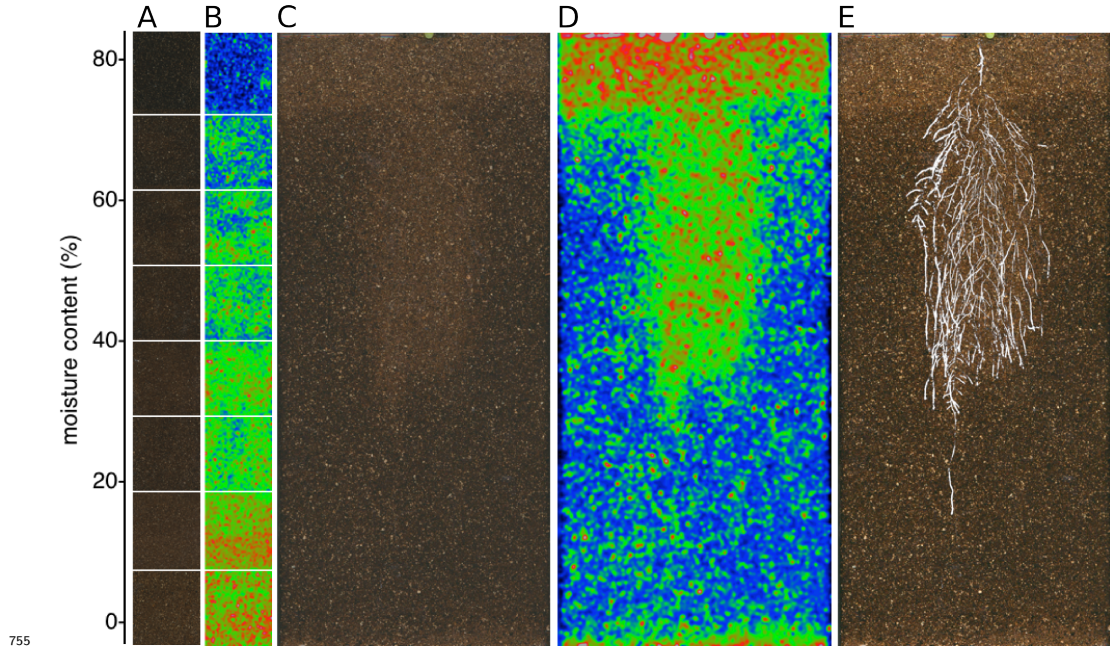


746

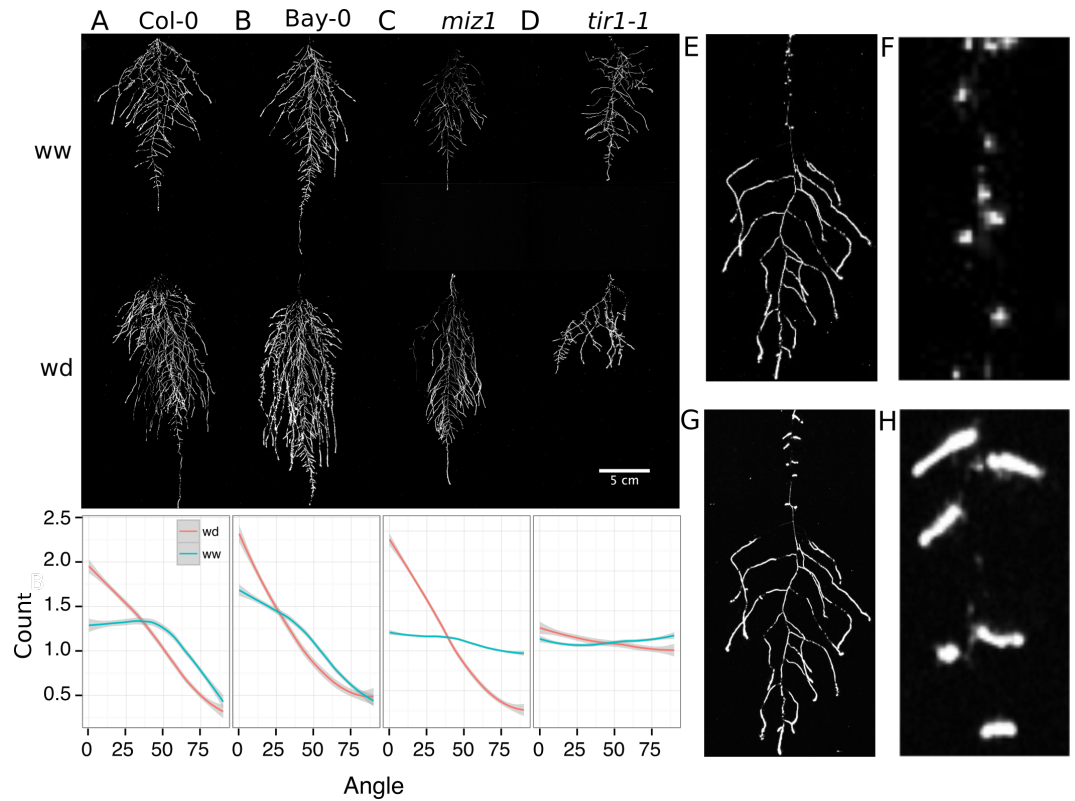
747 **Figure 4. Dual-color reporter visualization of structure and gene expression.**

748 Images of whole root systems (A,) or magnified portion of roots (C, F) at 22 DAS
749 expressing *ProDR5rev:LUC+* (green, A, B) or *ProZAT12:LUC* signal (green, C, D)with
750 skeletonized representation of roots generated using the *ProACT2:PpyRE8o* reporter
751 expression (in grey). E) Visualization of the results obtained by analyzing the ZAT12:LUC
752 image with the GLO-RIA Root Reporter module. Blue circles are proportional in size to

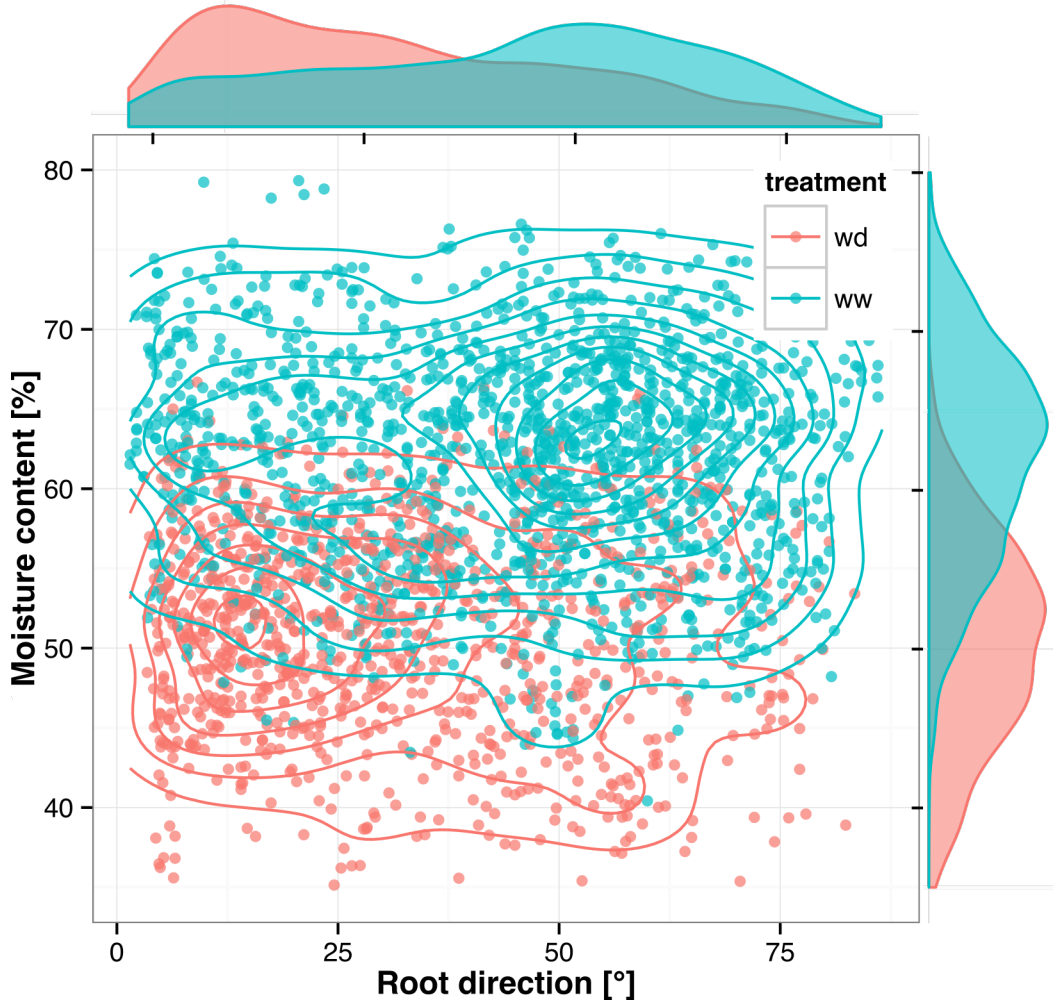
753 the ZAT12:LUC intensity value. Hovering over the points will reveal numerical values for
754 the ZAT12:LUC intensity



756 **Figure 5. Soil moisture and root architecture mapping in rhizotrons.** A) Com-
757 posite image showing regions of soil made from rhizotrons prepared with different moisture
758 levels. B) Differences in grey-scale intensity values were enhanced using a 16-color Look
759 Up Table (LUT). Brightfield image of soil in rhizotron (C) and converted using 16-color
760 LUT to enhance visualization of distribution of moisture (D) . E) Root system of a Bay-0
761 22 DAS and subjected to water deprivation since 13 DAS. Root system visualized using
762 luminescence and overlaid on brightfield image of soil in (C).

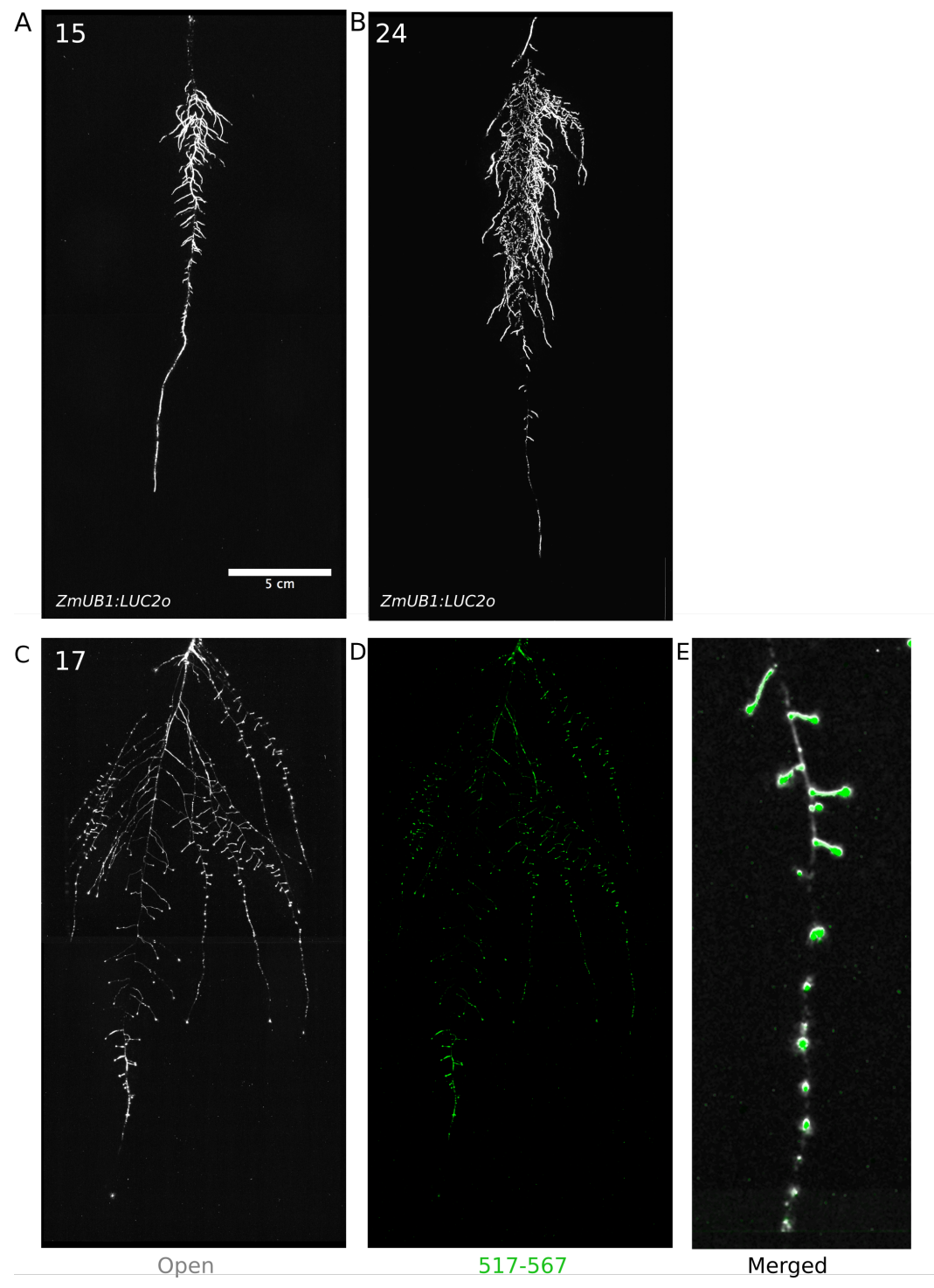


763
 764 **Figure 6. Study of effect of water deficit on root system architecture.** A-D)
 765 Root systems 22 DAS and exposed to water deficit 13 DAS onwards. Sample images of
 766 well watered (left panels) and water deficit (right panels) root systems treated from 13
 767 DAS and directionality (line graphs to left of images) for (A) Col-0 (B) Bay-0 (C) *miz1*
 768 mutant and (D) *tir1-1*. E) Root system of a 22 DAS plant exposed to water deprivation
 769 from 9 DAS onwards with magnified view of lateral root primordia (F). G) The same
 770 root as in (E) 24 hours after rewatering and magnified view of lateral root primordia (H).
 771 Kolmogorov-Smirnov test at $p < 0.001$ was used to compare directionality distributions
 772 between the different treatments and genotypes. A Local Polynomial Regression Fitting
 773 with 95% confidence interval (grey) was used to represent the directionality distribution
 774 curve. 0° is the direction of the gravity vector.



775

776 **Figure 7.** Relationship between local soil moisture content and root growth
 777 direction. Data quantified from the time lapse series shown in [Video 2](#). Density plots
 778 shown at periphery of graph for root direction (x-axis) and soil moisture (y-axis). 0° is
 779 the direction of the gravity vector. Data represents 2535 root tips measured in a series
 780 encompassing 10 time points.



782 **Figure 8:** Roots of *Brachypodium distachyon* transformed with *ProZmUB1:LUC2o* and

783 imaged at 15 (A) and 24 (B) DAS grown in control conditions. C) Open channel of 17
784 DAS tomato plant transformed with *ProeDR5rev:LUC2o* and *Pro35S:PPyRE8o* D) Green
785 channel showing only *ProeDR5rev:LUC2o* E) Amplification of the open and green channel
786 showing increased expression of *ProeDR5rev:LUC2o* reporter in early-stage lateral roots.

787 **Videos**

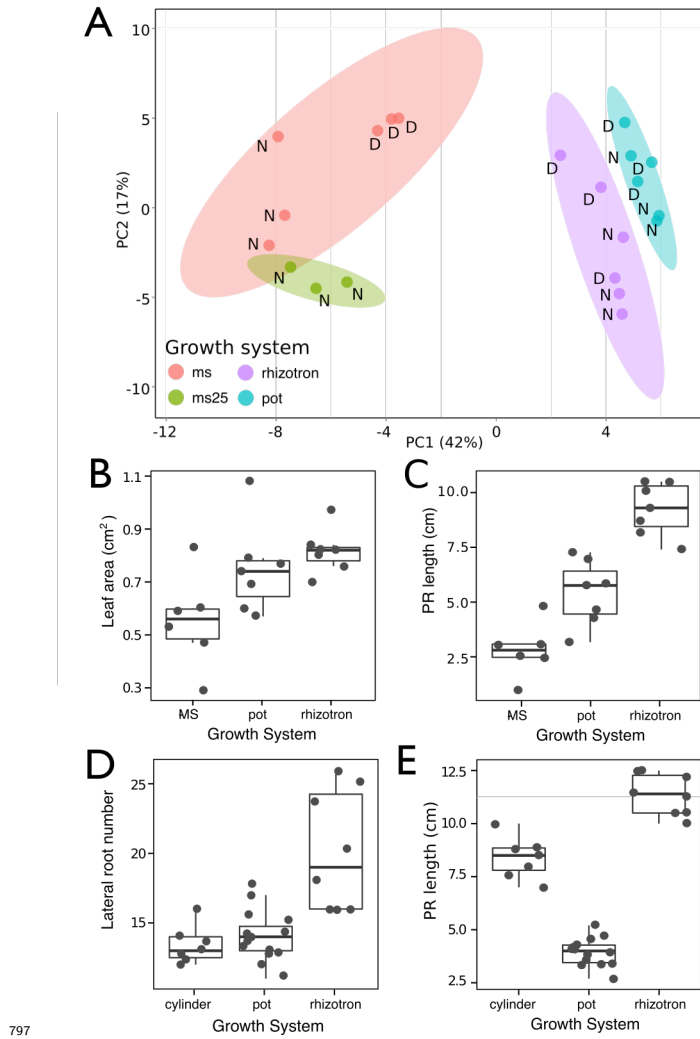
788 **Video 1** Time lapse from 11 to 21 DAS of a Col-0 plant expressing ProUBQ10:LUC2o
789 grown in control conditions

790 **Video 2** Time lapse from 16 to 24 DAS of Col-0 plants expressing *ProUBQ10:LUC2o*
791 growing in water deficient (left) and control (right) conditions. Plants were sown under
792 control conditions and water deficit treatment started 11 DAS. Images were taken every
793 day.

794

795 **Supplementary Material**

796 **Supplementary figures**



797 **Figure 1-figure supplement 1. Effect of different growth systems on plant biology.** A) Principal Components Analysis (PCA) score plot of a set of 76 genes analyzed by qPCR from root samples of plants grown in MS plates, pots, and rhizotrons. After 15 DAS three plants were collected at the end of the day (D) and three were collected at the end of the night (N). (ms = plant grown in full ms and 1% sucrose, ms25 = plants grown in 25% of full ms) B) Lateral root number and G) primary root length of 18 DAS plants grown in

804 30 cm tall cylinders, pots and rhizotrons, all with a volume of 100 cm³ (n = 6-12 plants).
805 D) Leaf area and E) primary root length of plants of the same age (15 DAS) as the ones
806 used for the qPCR experiment (n= 6-7). ANOVA analysis with p < 0.01 was used to test
807 significant differences between the different parameters.

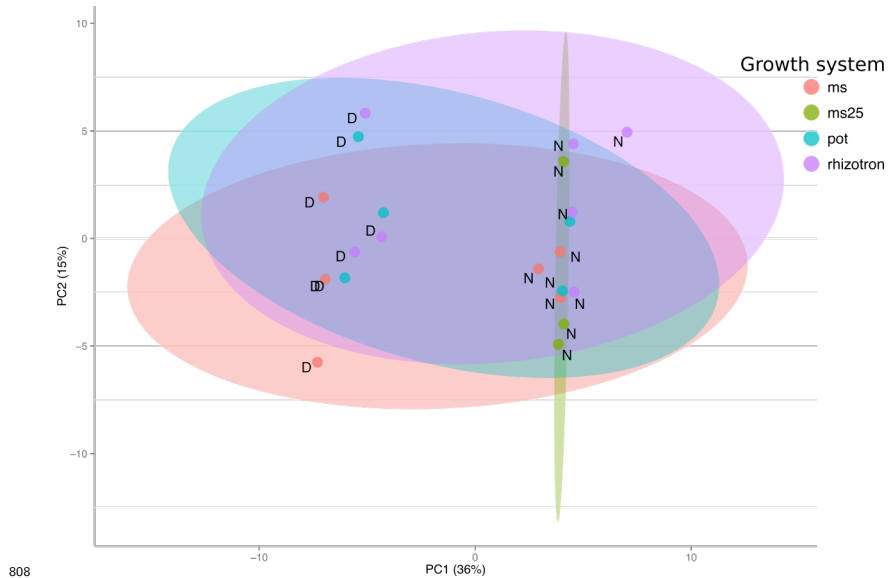
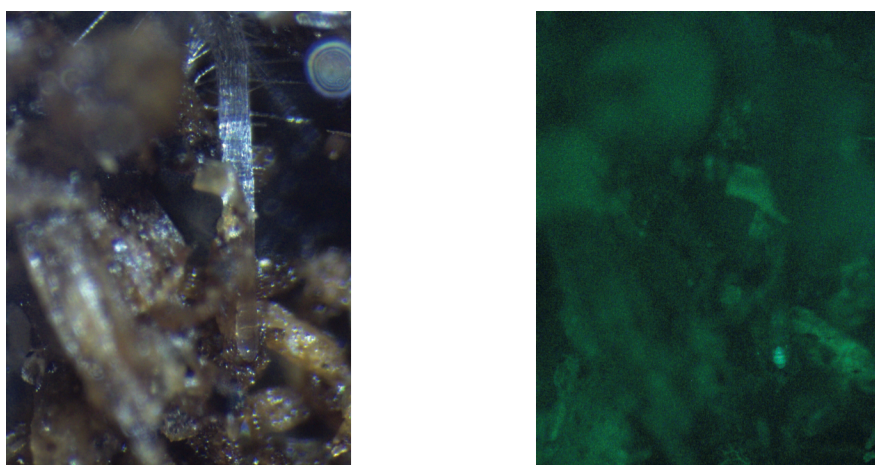
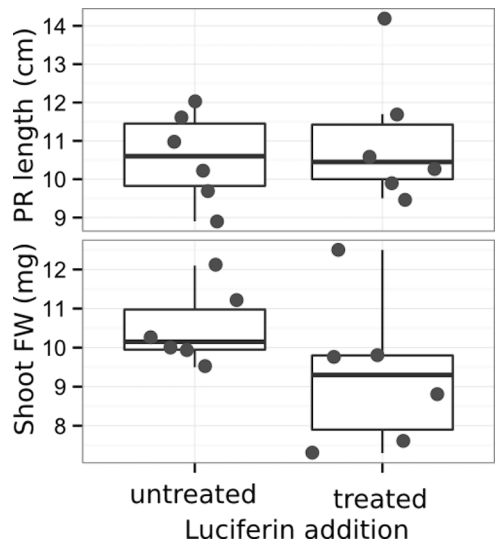


*Figure 1-figure supplement 2. PCA plot of shoots of the same samples analyzed in Figure 1. See Figure 1 for more details regarding experimental conditions used.



Brightfield GFP

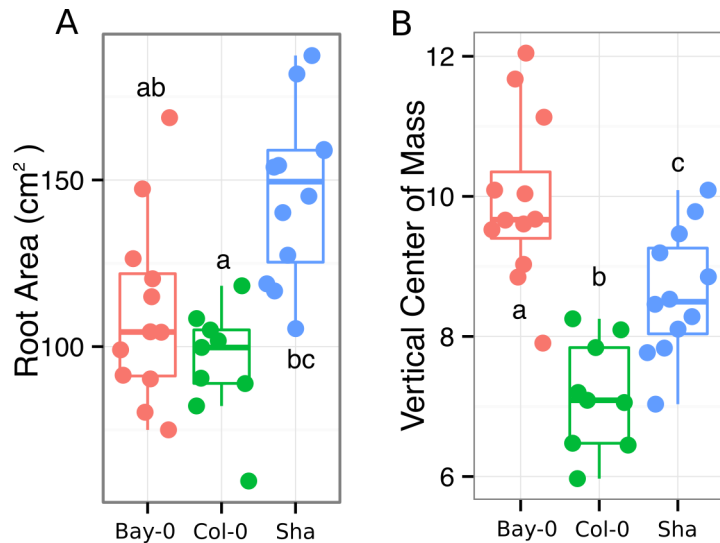
813 light (brightfield) or epifluorescence.



814

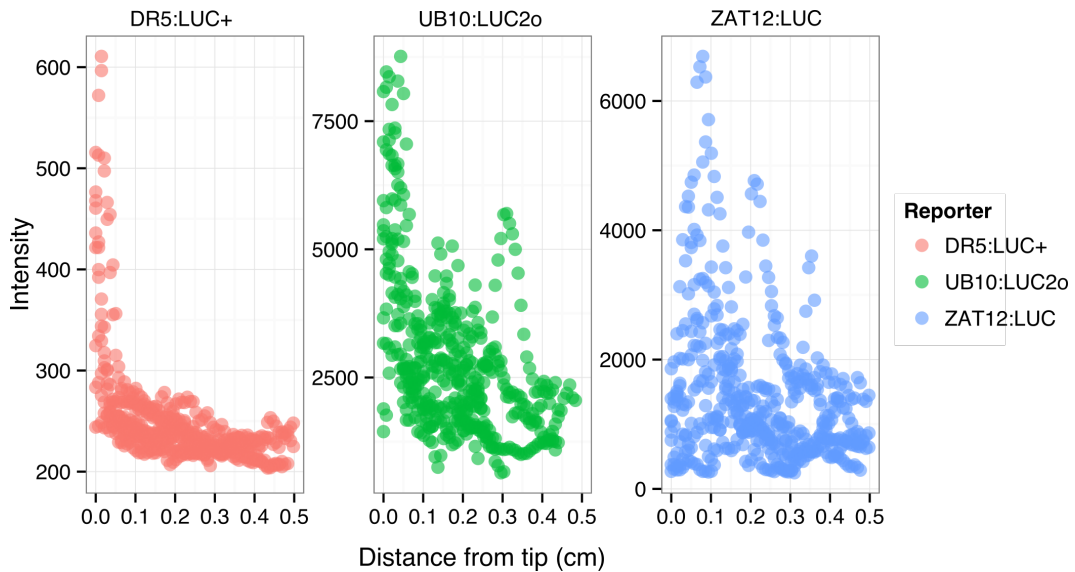
815 **Figure 1-figure supplement 4** Effect of luciferin addition on primary root length and
816 shoot size of 14 DAS seedlings that were either continuously exposed to 300 μ M luciferin
817 from 9 DAS after sowing or not.

818 **Figure 1-figure supplement data 1:** Two way ANOVA P-values comparing plants grown
819 in MS media vs. plants grown in soil (pots or rhizotrons) and plants collected at day or night.
820 We used p-value < 0.00065 threshold based on Bonferroni adjustment for multiple testing.



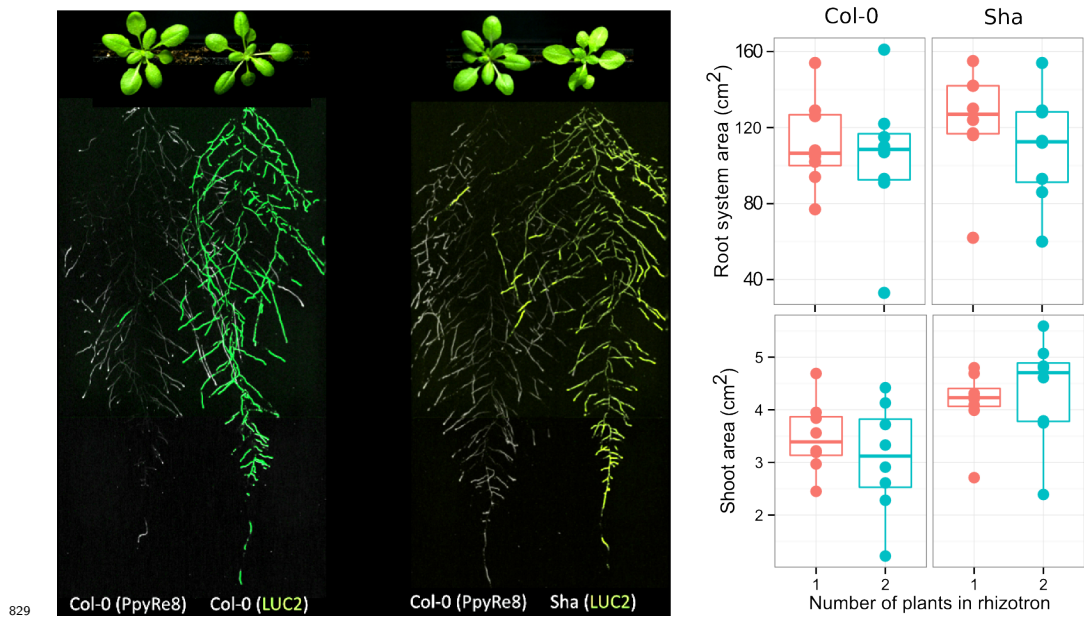
821 **Figure 3-figure supplement 1** A) root area, B) vertical center of mass of Bay-0, Col-0

823 and Sha accessions.



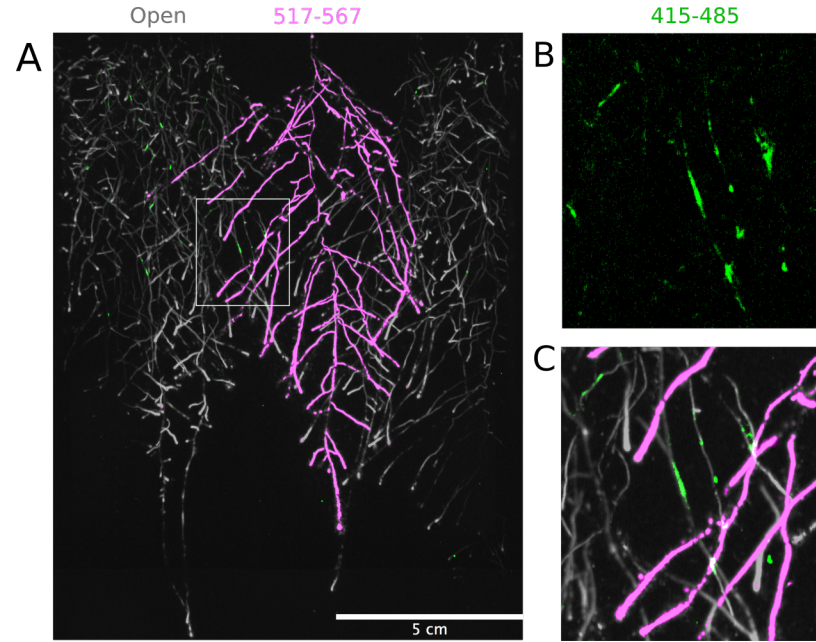
824

825 **Figure 4-figure supplement 1:** DR5:LUC+, UBQ10:LUC2o and ZAT12:LUC intensity
826 values along the root tip. Data was manually obtained by obtaining the intensity profile
827 of the first 0.5 cm from the root tip of individual lateral roots. Ten lateral roots for each
828 reporter were measured.

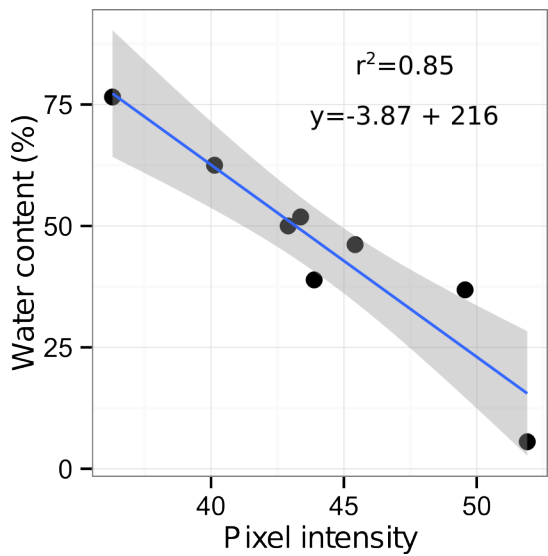


829 **Figure 4-figure supplement 2.** Images of plants at 22 DAS growing in the

831 same rhizotron and expressing different luciferases. A) Two Col-0 plants expressing
832 *ProUBQ10:LUC2o* and *ProACT2:PPyRE8o* B) Col-0 plant expressing *ProACT2:PPyRE8o*
833 and Sha plant expressing *ProUBQ10:LUC2o*.

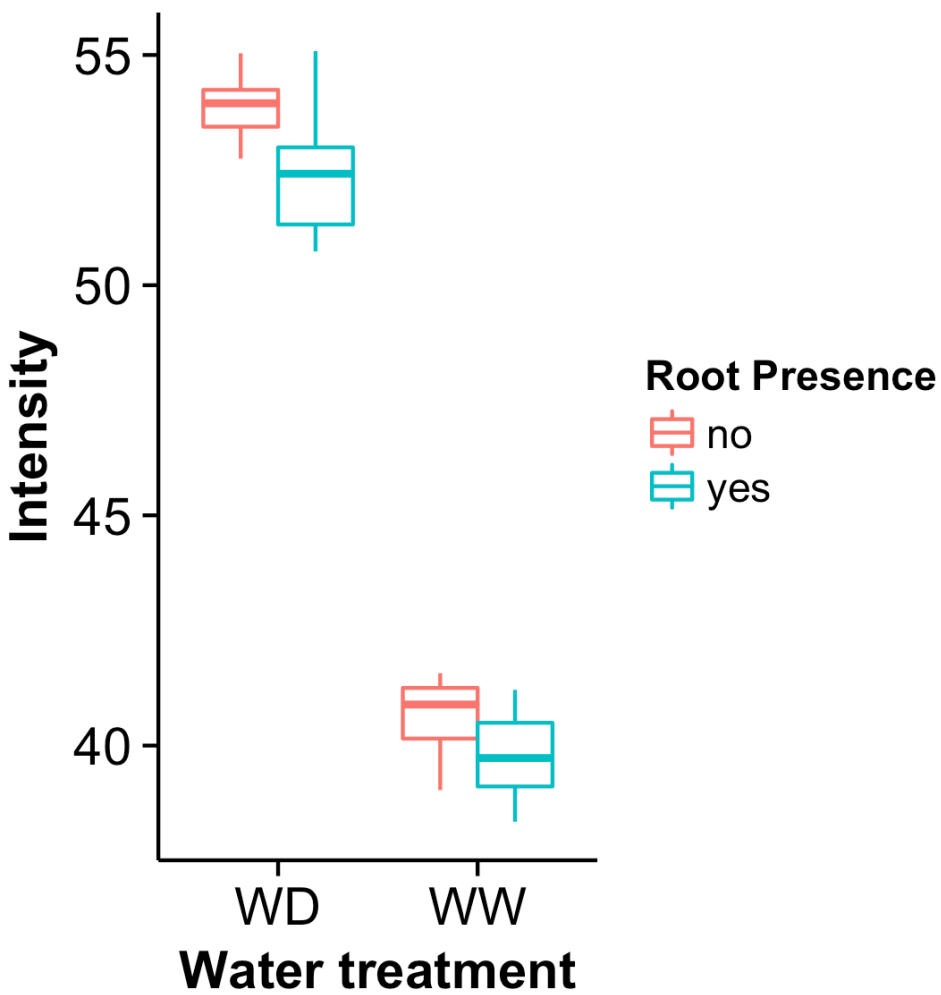


834
835 **Figure 4-figure supplement 3. Three-reporter-based analysis of root-root-**
836 **microbe interactions.** A) Image showing a 22 DAS *ProUBQ10:LUC2o* plant (magenta)
837 grown in the same rhizotron with *ProACT2:PpyRE8o* plants (grey). Plants were inoculated
838 with *Pseudomonas fluorescens* CH267 (green). Magnified portion of root systems colonized
839 by *Pseudomonas fluorescens* showing *P. fluorescences* (B) only or all three reporters
840 together (C).



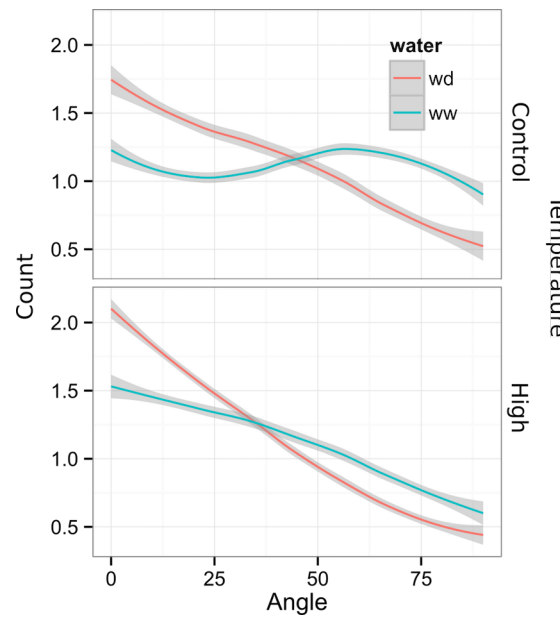
841

842 **Figure 5-figure supplement 1:** Moisture calibration curve. Rhizotrons with different
843 levels of moisture were prepared and scanned to obtain readings of pixel intensity. Soil from
844 rhizotrons was then weighed, dried down in an oven at 70 °C for 48 hours and percent water
845 content quantified.

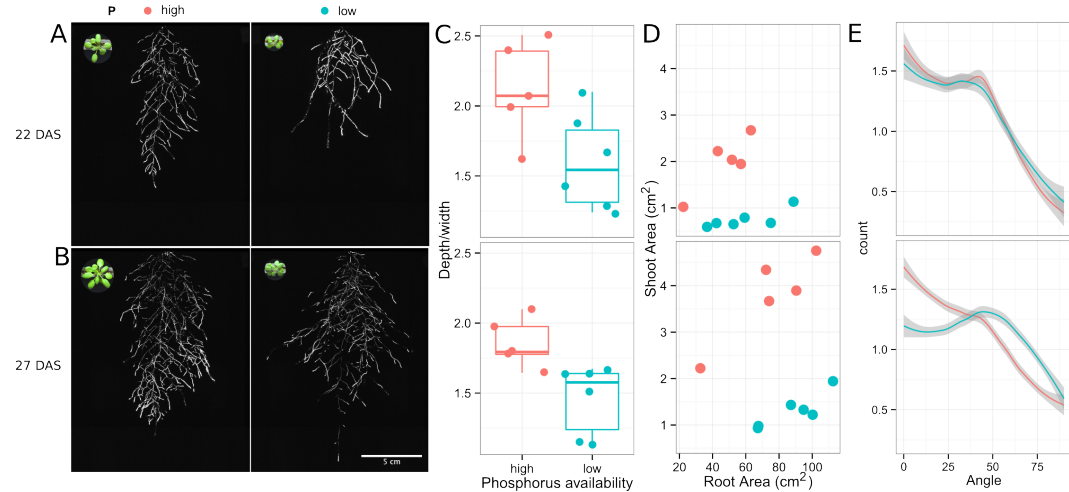


846

847 **Figure 5-figure supplement 2.** Comparison of soil intensity values between
848 areas of the rhizotron with or without the presence of roots, determined based
849 on luminescence data. Mean intensity values from 100 x 100 pixel squares samples of
850 both areas were obtained from 10 different rhizotrons. Wilcoxon test analysis with $p < 0.01$
851 was used to test significant differences between areas with our without root presence.

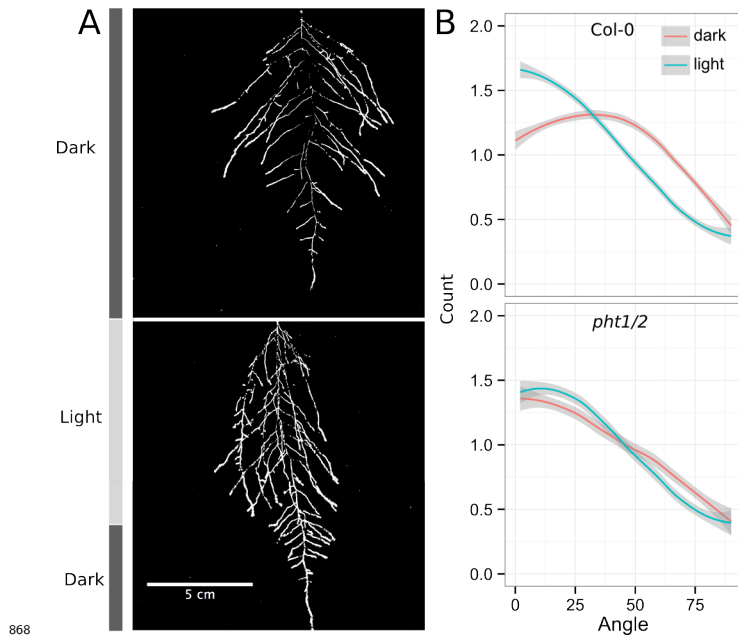


852
853 **Figure 6-figure supplement 1** Directionality analysis of roots of plants transferred to
854 water deprivation conditions after 9 DAS and kept 22 °C (control temperature) and 29 °C
855 (high temperature) until 22 DAS. (0° is the direction of the gravity vector).

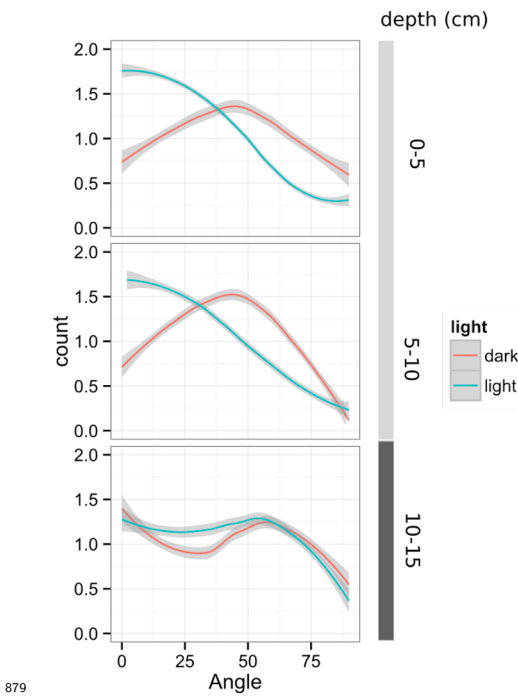


856
857 **Figure 6-figure supplement 2. Phosphorus deficiency response of root systems**
858 Shoot and root systems of *ProUBQ10:LUC2o* Col-0 plants growing in soil supplemented
859 with 1ml of 100 µM P-Alumina (left) and 0-P-Alumina (right) 22 (A) or 27 (B) DAS. C)
860 Root depth/width ratio of 22 (top) and 27 (bottom) DAS plants. D) Scatter-plot showing

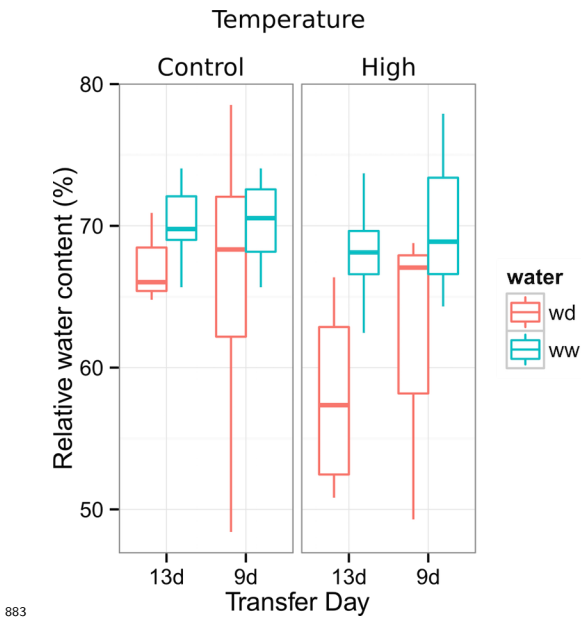
861 relationship between root and shoot system area at 22 (top) and 27 (bottom) DAS. E
 862 Root directionality distribution in plants 22 (top) and 27 (bottom) DAS. Anova analysis at
 863 $p < 0.01$ was used to compare depth/width ratios in P treatments. Kolmogorov-Smirnov
 864 test at $p < 0.001$ was used to compare directionality distributions between the different
 865 treatments. A Local Polynomial Regression Fitting with 95% confidence interval (grey)
 866 was used to represent the directionality distribution curve.(0° is the direction of the gravity
 867 vector).



868
 869 **Figure 6-figure supplement 3. Effect of light on root directionality.** A) Col-0
 870 root systems shielded (top) or light exposed (bottom). After 9 DAS the top third of the
 871 rhizotron was exposed to light (indicated on the side with a light grey bar) and plants were
 872 imaged at 20 DAS. B) Directionality analysis of root systems shielded (red) or exposed
 873 (green) to light for Col-0 (top panel) or *phot1/2* double mutant (bottom panel). Between
 874 4 and 6 plants were analyzed per treatment. ANOVA analysis at $p < 0.01$ was used to
 875 compare depth/width ratios in P treatments. Kolmogorov-Smirnov test at $p < 0.001$ was
 876 used to compare directionality distributions between the different treatments. A Local
 877 Polynomial Regression Fitting with 95% confidence interval (grey) was used to represent
 878 the directionality distribution curve.(0° is the direction of the gravity vector).

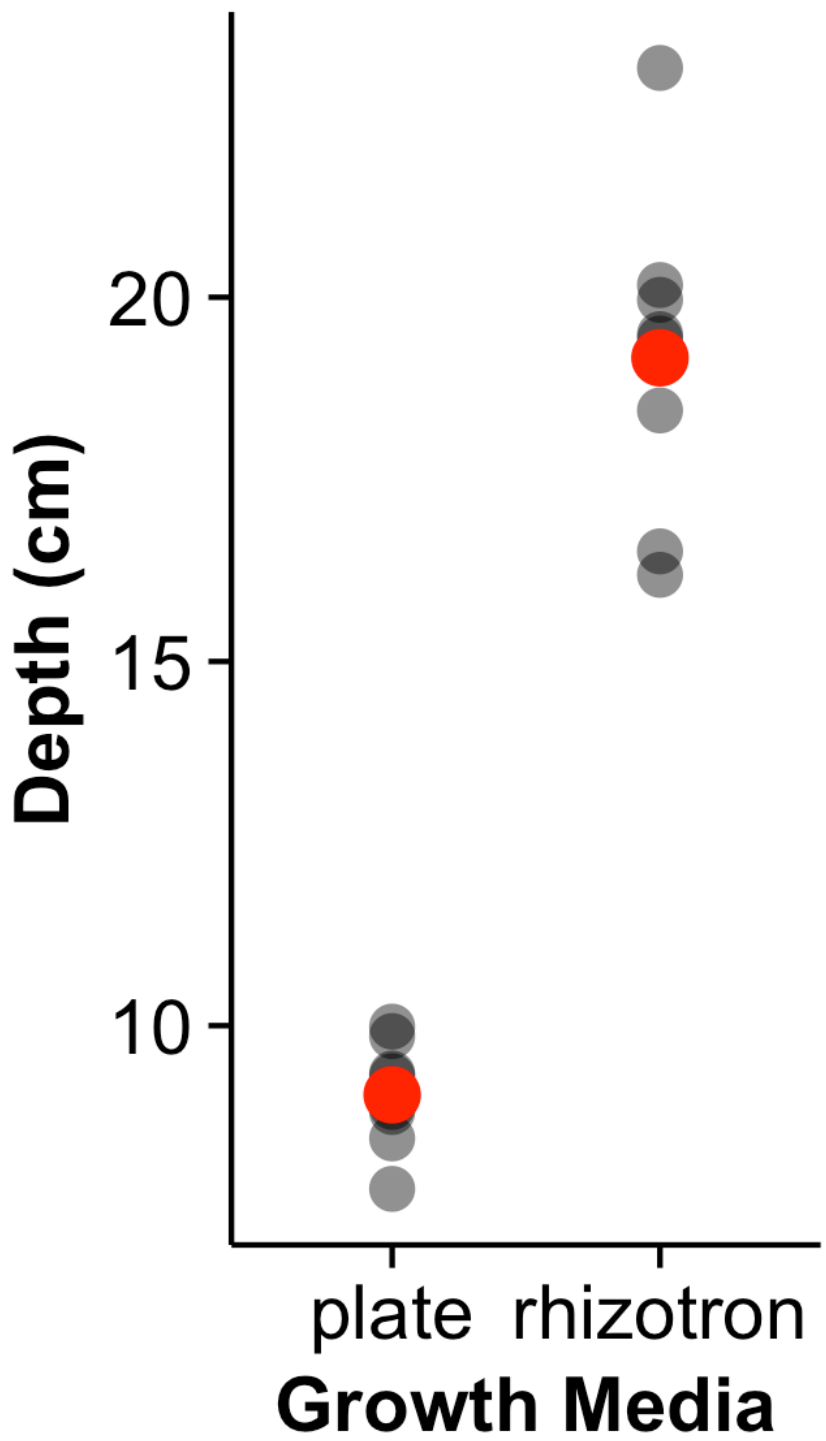


879 **Figure 6-figure supplement 4** Plots showing output of directionality analysis performed
 880 at different depths (0-5, 5-10, 10-15 cm) in rhizotrons exposed to light or kept in the dark.
 881 (0° is the direction of the gravity vector).



883 **Figure 6-figure supplement 5.** Leaf relative water content of 23 DAS plants that

⁸⁸⁵ were subjected to water deprivation (WD) after 9 or 13 DAS or kept under
⁸⁸⁶ well watered (WD) conditions. At 9 DAS half of the plants were kept under control
⁸⁸⁷ temperature conditions (22 °C) and the other half transferred to a 29 °C (high) chamber. n
⁸⁸⁸ = 6-8 plants.



890 **Figure 8-figure supplement 1** Depth of the primary root of Brachypodium plants grown
891 in rhizotrons or on gel-based media (n=8-11).

892 **Supplementary material**

893 **Supplemental Material 1**

894 Blueprints of the holders, clear sheets and spacers needed to built the rhizotrons. Additional
895 details are provided in the materials and methods. Files are provided in Adobe Illustrator
896 .ai and Autocad .dxf formats.

897 **Supplemental Material 2**

898 Primers used in the qPCR experiment.

899 **Supplemental Material 3**

900 Vector maps of all the constructs used in this work.

901 **Source data files**

902 Source data files used for building the following figures are provided:

903 figure_1D.csv
904 figure_1_figure_supplement_1A-B.csv
905 figure_1_figure_supplement_1C_D.csv
906 figure_1_figure_supplement_1E-F.csv
907 figure_1_figure_supplement_2.csv
908 figure_1_figure_supplement_3.csv
909 figure_2C.csv
910 figure_2D.csv
911 figure_3D.csv
912 figure_3E.csv
913 figure_3F-G_1.csv
914 figure_3F-G_2.tps

915 figure_3_figure_supplement_1A-B.csv
916 figure_4G_reporter.csv
917 figure_4G_root_segment.csv
918 figure_4_figure_supplement_1.csv
919 figure_4_figure_supplement_2.csv
920 figure_5_figure_supplement_1.csv
921 figure_6_A-D.csv
922 figure_6_figure_supplement_2-C-D.csv
923 figure_6_figure_supplement_2-E.csv
924 figure_6_figure_supplement_3.csv
925 figure_6_figure_supplement_4.csv
926 figure_6_figure_supplement_5.csv
927 figure_7.csv
928 figure_8_figure_supplement_1.csv

929

930 References

- 931 1.Dinneny, J. R. *et al.* Cell identity mediates the response of *Arabidopsis* roots to abiotic
932 stress. *Science* **320**, 942–945 (2008).
- 933 2.Duan, L. *et al.* Endodermal ABA Signaling Promotes Lateral Root Quiescence during
934 Salt Stress in Arabidopsis Seedlings. *Plant Cell* **25**, 324–341 (2013).
- 935 3.Lynch, J. P. & Wojciechowski, T. Opportunities and challenges in the subsoil: pathways
936 to deeper rooted crops. *J. Exp. Bot.* **66**, 2199–2210 (2015).
- 937 4.Brady, N. C. & Weil, R. R. *Elements of the nature and properties of soils*. (Prentice Hall,
938 2009).
- 939 5.Bao, Y. *et al.* Plant roots use a patterning mechanism to position lateral root branches
940 toward available water. *Proc Natl Acad Sci* **111**, 9319–9324 (2014).

- 941 6.Tabata, R. *et al.* Perception of root-derived peptides by shoot LRR-RKs mediates systemic
942 N-demand signaling. *Science* **346**, 343–346 (2014).
- 943 7.Rosquete, M. R. *et al.* An Auxin Transport Mechanism Restricts Positive Orthogravit-
944 ropicism in Lateral Roots. *Current Biology* **23**, 817–822 (2013).
- 945 8.Uga, Y. *et al.* Control of root system architecture by DEEPER ROOTING 1 increases
946 rice yield under drought conditions. *Nat. Genet.* **45**, 1097–1102 (2013).
- 947 9.Postma, J. A. & Lynch, J. P. The optimal lateral root branching density for maize depends
948 on nitrogen and phosphorus availability. *Plant Physiol.* **166**, 590–602 (2014).
- 949 10.Schneider, C. A., Rasband, W. S. & Eliceiri, K. W. NIH Image to ImageJ: 25 years of
950 image analysis. *Nature methods* **9**, 671–675 (2012).
- 951 11.Meijon, M., Satbhai, S. B., Tsuchimatsu, T. & Busch, W. Genome-wide association study
952 using cellular traits identifies a new regulator of root development in. *Nat. Genet.* **46**, 77–81
953 (2013).
- 954 12.Hara-Miyauchi, C. *et al.* Bioluminescent system for dynamic imaging of cell and animal
955 behavior. *Biochem. Biophys. Res. Commun.* **419**, 188–193 (2012).
- 956 13.Emami, S., Yee, M.-C. & Dinneny, J. R. A robust family of Golden Gate Agrobacterium
957 vectors for plant synthetic biology. *Front. Plant Sc.* **4**, 339 (2013).
- 958 14.Hall, M. P. *et al.* Engineered Luciferase Reporter from a Deep Sea Shrimp Utilizing a
959 Novel Imidazopyrazinone Substrate. *ACS chemical biology* **7**, 1848–1857 (2012).
- 960 15.Ristova, D. *et al.* RootScape: a landmark-based system for rapid screening of root
961 architecture in Arabidopsis. *Plant Physiology* **161**, 1086–1096 (2013).
- 962 16.Lobet, G. *et al.* Root System Markup Language: toward a unified root architecture
963 description language. *Plant Physiol.* **167**, 617–627 (2015).
- 964 17.Moreno-Risueno, M. A. *et al.* Oscillating gene expression determines competence for
965 periodic *Arabidopsis* root branching. *Science* **329**, 1306–1311 (2010).

- 966 18.Miller, G. *et al.* The plant NADPH oxidase RBOHD mediates rapid systemic signaling
967 in response to diverse stimuli. *Science Signaling* **2**, ra45 (2009).
- 968 19.Haney, C. H., Samuel, B. S., Bush, J. & Ausubel, F. M. Associations with rhizosphere
969 bacteria can confer an adaptive advantage to plants. *Nature Plants* **1**, 15051 (2015).
- 970 20.Mandoli, D. F., FORD, G. A., WALDRON, L. J., NEMSON, J. A. & Briggs, W. R. Some
971 spectral properties of several soil types: implications for photomorphogenesis*. *Plant Cell*
972 *Environ.* **13**, 287–294 (1990).
- 973 21.Galen, C., Rabenold, J. J. & Liscum, E. Functional ecology of a blue light photoreceptor:
974 effects of phototropin-1 on root growth enhance drought tolerance in *Arabidopsis thaliana*.
975 *New Phytol.* **173**, 91–99 (2007).
- 976 22.Moni, A., Lee, A. Y., Briggs, W. R. & Han, I. S. The blue light receptor Phototropin 1
977 suppresses lateral root growth by controlling cell elongation. *Plant Biology* 34–40 (2014).
- 978 23.Yokawa, K., Kagenishi, T. & Baluška, F. Root photomorphogenesis in laboratory-
979 maintained *Arabidopsis* seedlings. *Trends Plant Sci.* **18**, 117–119 (2013).
- 980 24.Lobell, D. B. *et al.* Greater Sensitivity to Drought Accompanies Maize Yield Increase in
981 the U.S. Midwest. *Science* **344**, 516–519 (2014).
- 982 25.Ort, D. R. & Long, S. P. Limits on Yields in the Corn Belt. *Science* **344**, 484–485 (2014).
- 983 26.Pacheco-Villalobos, D. & Hardtke, C. S. Natural genetic variation of root system archi-
984 tecture from *Arabidopsis* to *Brachypodium*: towards adaptive value. *Philosophical Trans-
985 actions of the Royal Society of London B: Biological Sciences* **367**, 1552–1558 (2012).
- 986 27.Watt, M., Schneebeli, K., Dong, P. & Wilson, I. W. The shoot and root growth of
987 *Brachypodium* and its potential as a model for wheat and other cereal crops. *Functional
988 Plant Biol.* **36**, 960–969 (2009).
- 989 28.Mann, D. G. J. *et al.* Gateway-compatible vectors for high-throughput gene functional
990 analysis in switchgrass (*Panicum virgatum* L.) and other monocot species. *Plant Biotechnol.
991 J.* **10**, 226–236 (2012).

- 992 29.Pacheco-Villalobos, D., Sankar, M., Ljung, K. & Hardtke, C. S. Disturbed Local
993 Auxin Homeostasis Enhances Cellular Anisotropy and Reveals Alternative Wiring of
994 Auxin-ethylene Crosstalk in *Brachypodium distachyon* Seminal Roots. *PLoS Genet* **9**,
995 e1003564 (2013).
- 996 30.Buer, C. S., Wasteneys, G. O. & Masle, J. Ethylene modulates root-wave responses in
997 *Arabidopsis*. *Plant Physiology* **132**, 1085–1096 (2003).
- 998 31.Blossfeld, S., Schreiber, C. M., Liebsch, G., Kuhn, A. J. & Hinsinger, P. Quantitative
999 imaging of rhizosphere pH and CO₂ dynamics with planar optodes. *Annals of Botany* **112**,
1000 267–276 (2013).
- 1001 32.Shaw, S. L. & Ehrhardt, D. W. Smaller, Faster, Brighter: Advances in Optical Imaging
1002 of Living Plant Cells. *Annu. Rev. Plant Biol.* **64**, 351–375 (2013).
- 1003 33.Barr, H. & Weatherley, P. A re-examination of the relative turgidity technique for esti-
1004 mating water deficit in leaves. *Aust. J. Biol. Sci* **15**, 413–428 (1962).
- 1005 34.Grapov, D. DeviumWeb: Dynamic Multivariate Data Analysis and Visualization Plat-
1006 form.
- 1007 35.Branchini, B. R. *et al.* Red-emitting luciferases for bioluminescence reporter and imaging
1008 applications. *Analytical Biochemistry* **396**, 290–297 (2010).
- 1009 36.Branchini, B. R. *et al.* Thermostable red and green light-producing firefly luciferase
1010 mutants for bioluminescent reporter applications. *Analytical Biochemistry* **361**, 253–262
1011 (2007).
- 1012 37.Lane, M. C., Alteri, C. J., Smith, S. N. & Mobley, H. L. T. Expression of flagella is
1013 coincident with uropathogenic *Escherichia coli* ascension to the upper urinary tract. *Proc.
1014 Natl. Acad. Sci. U.S.A.* **104**, 16669–16674 (2007).
- 1015 38.Ruegger, M. *et al.* The TIR1 protein of *Arabidopsis* functions in auxin response and is
1016 related to human SKP2 and yeast grr1p. *Genes Dev* **12**, 198–207 (1998).
- 1017 39.Moriwaki, T. *et al.* Hormonal Regulation of Lateral Root Development in *Arabidopsis*

- 1018 Modulated by MIZ1 and Requirement of GNOM Activity for MIZ1 Function. *Plant Physiol.*
1019 **157**, 1209–1220 (2011).
- 1020 40.Vogel, J. & Hill, T. High-efficiency Agrobacterium-mediated transformation of Brachy-
1021 podium distachyon inbred line Bd21-3. *Plant Cell Rep* **27**, 471–478 (2008).
- 1022 41.Covington, M. F. & Harmer, S. L. The Circadian Clock Regulates Auxin Signaling and
1023 Responses in Arabidopsis. *Plos Biol* **5**, e222 (2007).
- 1024 42.Lindeboom, J. J. *et al.* A Mechanism for Reorientation of Cortical Microtubule Arrays
1025 Driven by Microtubule Severing. *Science* **342**, 1245533–1–1245533–11 (2013).
- 1026 43.Chitwood, D. H. *et al.* A modern ampelography: a genetic basis for leaf shape and
1027 venation patterning in grape. *Plant Physiology* **164**, 259–272 (2014).
- 1028 44.Iwata, H. & Ukai, Y. SHAPE: a computer program package for quantitative evaluation of
1029 biological shapes based on elliptic Fourier descriptors. *The Journal of Heredity* **93**, 384–385
1030 (2002).
- 1031 45.R Core Team. *R: A language and environment for statistical computing*. (R Foundation
1032 for Statistical Computing, 2014). at <<http://www.R-project.org/>>
- 1033 46.Wickham, H. *Tidyr: Easily tidy data with spread() and gather() functions*. (2014). at
1034 <<http://CRAN.R-project.org/package=tidyr>>
- 1035 47.Auguie, B. *GridExtra: Functions in grid graphics*. (2012). at <<http://CRAN.R-project.org/>>/
1036 *package=gridExtra*>
- 1037 48.Dryden, I. L. *Shapes: Statistical shape analysis*. (2013). at <<http://CRAN.R-project.org/>>/
1038 *package=shapes*>
- 1039 49.Adams, D. & Otarola-Castillo, E. Geomorph: An r package for the collection and analysis
1040 of geometric morphometric shape data. *Methods in Ecology and Evolution* **4**, 393–399 (2013).
- 1041 50.Wickham, H. *Ggplot2: Elegant graphics for data analysis*. (Springer New York, 2009).
1042 at <<http://had.co.nz/ggplot2/book>>

¹⁰⁴³ 51.Wilke, C. O. *cowplot: Streamlined Plot Theme and Plot Annotations for ggplot2*. (2015).

¹⁰⁴⁴ at <<http://cran.r-project.org/web/packages/cowplot/index.html>>